ISSN 2693-0935

Ancient TL

A periodical devoted to Luminescence and ESR dating

Department of Physics, East Carolina University, 1000 East 5th Street, Greenville, NC 27858, USA
http://ancienttl.org

December 2023, Volume 41 No.2

Ancient TL

Started by the late David Zimmerman in 1977

Ancient TL

A safe procedure for HF etching as part of sample preparation for luminescence dating

Galina Faershtein[1]* and Naomi Porat[2]

[1] Department of Earth and Planetary Sciences, Weizmann Institute of Science, Rehovot, Israel
[2] Geological Survey of Israel, Jerusalem, Israel

*Corresponding Author: galina.faershtein@weizmann.ac.il

Received: June 22, 2023; in final form: October 1, 2023

Abstract

This paper presents a protocol for safe quartz etching with hydrofluoric (HF) acid as part of sample preparation for luminescence dating. Concentrated HF is extremely hazardous and can cause severe burns and poisoning, even leading to death. Generally, in order to avoid exposure to light and bleaching, HF etching is performed in a dark laboratory under weak orange-red light in wide-open beakers. Handling HF in open beakers in the dark could result in unfortunate accidents due to unintentional spillage. The presented protocol avoids these two main safety issues – working with open beakers and under poor lighting. The samples are etched inside black opaque bottles with narrow openings so that the procedure can be safely performed in comfortable light levels. To validate the harmlessness of the laboratory environmental light, bleaching experiments of quartz were conducted under the same conditions as the protocol. These showed that no bleaching occurred during this procedure.

Keywords: Hydrofluoric acid, Quartz-etching

1. Introduction

Extraction of quartz and alkali-feldspar (KF) grains for luminescence dating includes etching with hydrofluoric (HF) acid (Aitken, 1985; Wintle, 1997), which is highly corrosive. Different laboratories have varying practices, but generally, quartz grains are etched with concentrated HF (40 – 48 %) for at least 40 minutes. This step is essential for dissolving feldspars, removing clay or iron oxide coating on the grains, and etching the outer rim of the quartz grains affected by alpha particles during burial. Regarding KF etching, the procedure is less uniform across laboratories. As feldspar is affected much faster by the HF, the grains are usually etched with diluted acid (10 %) for various durations (0 – 40 min). Porat et al. (2015) investigated the KF grain size reduction by different HF treatments and suggested etching the feldspars with 10 % HF for 10 min.

HF acid is extremely hazardous as it can cause severe burns and poisoning (Bertolini, 1992; Wang et al., 2014), even leading to death (Muriale et al., 1996). Therefore, it should be handled with extra caution, and any work with it should be carried out in designated fume hoods. For safety, one usually wears additional protective clothing such as a lab coat, closed shoes, protective goggles, suitable gloves, a rubber apron, and rubber sleeves.

Generally, in order to avoid exposure to light and bleaching, the HF etching procedure is performed in a dark laboratory under weak orange-red light in wide open beakers using access HF acid. Even when taking all precautions, handling HF in open beakers under insufficient light could result in unfortunate accidents due to unintentional spillage.

The luminescence laboratory at the Geological Survey of Israel (GSI) developed a protocol for HF etching that avoids the two main safety issues – open beakers and poor lighting. The protocol was tested on samples that had also been prepared in other laboratories using more conventional protocols, such as coastal sediment from the Skagen peninsula, Denmark, and no difference was found in the measured D_e values (Murray et al., 2015). Here, we describe the safe procedure for HF etching as part of sample preparation for luminescence dating.

Figure 1. Setting of the HF etching procedure within a chemical fume hood. a) The HF is transferred from the HF bottle to the sample bottles through the peristaltic pump. The cup connected to the pump tube (sample closest to the pump) is moved from one sample to the next. b) The bottle cap that is moved from sample to sample has two holes, one with the exact diameter of the tube, where it is placed, and a smaller one to release air. c) After 40 minutes of soaking, the spent acid is carefully poured into a waste bottle. Note that the sample will settle in the shoulder of the bottle.

2. Procedure description

The HF etching protocol uses 250 mL black, light-tight polyethylene bottles with caps and a narrow opening that prevents any light from reaching the bottom of the bottle (Fig. 1). About 3 g from each sample is weighed into a bottle in the dark, and the cap is replaced. From this step, the procedure is continued with comfortable light levels within a chemical fume hood. If there are no windows introducing daylight into the preparation laboratory or white light lamps, this procedure can be carried out at any chemistry laboratory. A fixed amount of HF (5 mL per 1 g quartz) is pumped into the bottles one after the other using a calibrated peristaltic pump and a timer. Each sample is soaked for 40 minutes in the HF. During this time, the bottles are repeatedly shaken every few minutes. After 40 minutes, the spent acid is poured out into a designated waste disposal container (Fig. 1), and the bottle is filled with water for a first rinse. After about a minute, this first rinse is carefully poured out, and water is added for a second rinse, after which the bottle is closed and ready to be returned to the dark lab. There, each sample is transferred to a corresponding beaker for three additional rinsing steps. Then, the samples are placed in 16 % HCl overnight to dissolve fluorides. The next day, the samples are thoroughly rinsed and dried, ready for measurements. For safety reasons and convenience, this protocol is carried out by two people, although one can easily do it alone.

Peristaltic pumps are used in geochemistry laboratories to transfer solutes into analytical instruments. Their advantage is that they are quiet, can be adjusted to pumping exact volumes over a given time, and when turned off, the pipe with the acid does not drip, so that the HF does not drip in the few seconds, it takes to transfer the pipe from bottle to bottle. Before starting, one should calibrate the volume of the liquid pumped over one minute (no need to use HF for that; water is just as good). Hypothetically, the pump can work faster and pump the required HF volume over less time so that more samples can be etched in a single batch. Depending on the available pumping rate and amount of feldspar contamination, each laboratory can work out their batch so

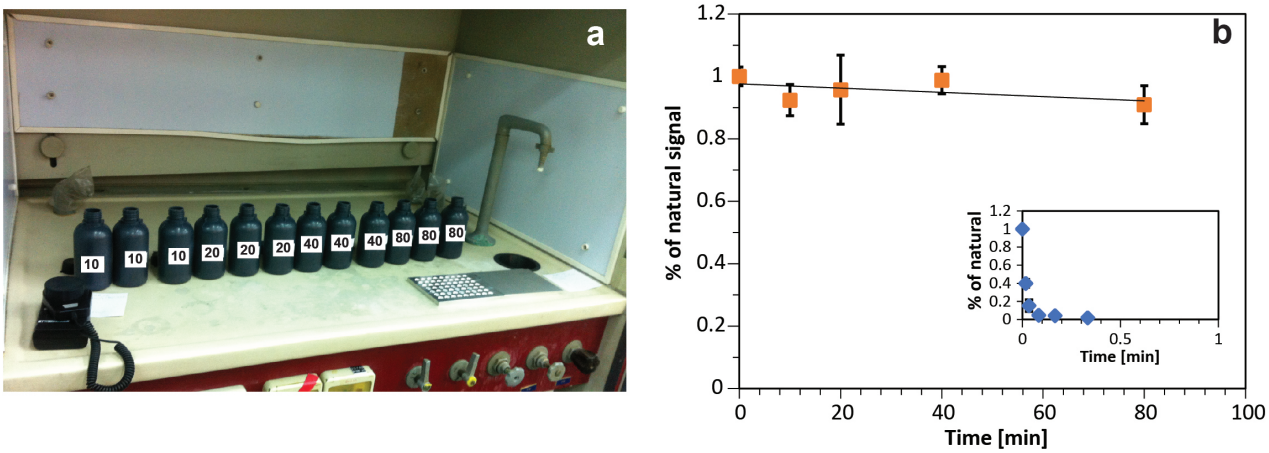

Figure 2. Quartz bleaching experiment inside the black bottles used for HF etching. a) The experiment setup within the fume hood. One disc is settled in each bottle. The numbers on the bottles are the bleaching durations in minutes. b) The experiment results. The inset–bleaching experiment results in full sunlight.

that it would finish well under 40 minutes (or the laboratory's standard etching time).

The amount of quartz etched from each sample is usually 3 g – if available – or less. Three grams were found to be sufficient even if half the amount was lost by dissolution and some spillage during rinsing. Even if only 1 g remains, one can make more than 100 x 9 mm aliquots or 1000 x 2 mm aliquots. Smaller quantities require more careful handling, but even 200 mg of final weight is sufficient for ordinary samples. Smaller amounts of quartz mean less HF used, which is beneficial on all accounts.

Following the recommendations of Bell & Zimmerman (1978) and Aitken (1985), it is postulated to etch the outer 10 mm of the quartz grains to neglect the alpha radiation from the dose rate evaluation. For etching quartz, about 5 mL of HF for each gram of sample is sufficient. Adding more acid does not remove more than the required 10 µm (Porat et al., 2015). However, if large amounts of feldspars are present (e.g. when samples are treated to only a single density separation of 2.62 g cm^{-3}), the volume of HF should be doubled or even tripled to allow the complete dissolution of feldspars.

Before the etching procedure, it is essential to ensure that all the carbonates in the sample have been dissolved in advance by HCl. Any remaining $CaCO_3$ will strongly react with the HF and form hard-to-dissolve calcium fluorides. Porat et al. (2015) showed that even after complete carbonate dissolution, some fluorides are still formed during the HF etching process. The source of the Ca is probably from plagioclase in the sample. Nevertheless, these dissolve later in the following HCl treatment (Porat et al., 2015).

Here is a working example from the GSI for a 40 minutes etching (procedure video is available at `https://youtu.be/lZbMpKDgf-s`): There are 18 samples in a batch. Three grams of quartz are weighed from each sample. Most samples contain little feldspars, so 15 ml of HF (5 mL x 3 g) is sufficient. The pump is set for a flow of 10 mL per minute, so the pumping time is 1.5 min. With 15 – 20 seconds added for moving from sample to sample, it takes roughly 1.75 min per sample. This works out fine as the filling time for the 18 samples will be 1.75 min x 18, i.e. 32 minutes. Thus, pumping HF to the last sample ends about 8 minutes before the first sample needs to be rinsed, leaving time for the unexpected.

HF etching affects grain's morphology differently, depending on their content, structure, and sedimentary maturity (Bell & Zimmerman, 1978; Porat et al., 2015). Duval et al. (2018) recommended that each laboratory evaluate the outer rind thickness etched by their procedure. For the presented procedure, it was reported on removal of 10 – 50 µm from the quartz rims depending on the sedimentological maturity and mineral purity (Porat et al., 2015). For quartz grains of mature sedimentary origin, 10 µm were etched as desired. For grains from immature sources, the grain size was reduced by up to 50 µm, primarily due to breakage along etched plains. Therefore, after the HF etching, for immature sediments, it is recommended to sieve at 20 µm below the original grain size to get rid of the broken grains.

3. Bleaching experiments

As the procedure is performed under regular laboratory fluorescent light, it was essential to ensure that the luminescence signal of the samples does not undergo any bleaching. In order to do so, a bleaching experiment was conducted. Five mm aliquots of purified quartz (sample FGA-26 from Faershtein et al. 2016) were placed in empty, open 250 mL black bottles, used for the HF etching procedure, for different periods of time up to 80 min, with the fluorescent lights turned on (Fig. 2a). Three aliquots were used for each bleaching duration (each aliquot was placed in a separate bottle). The bottles were placed 25 cm from the fume hood opening. The average light intensity next to the bot-

tles was measured at 170 lux. For comparison, a bleaching experiment was also conducted for the quartz grains in full sunlight (light intensity was measured at 57000 lux).

The experiment indicates that after 80 min inside open black bottles, the OSL signal is reduced by up to 10 % of the original signal (Fig. 2b). Some of the aliquots are not bleached at all. One of the aliquots that was bleached for 10 min showed a bleaching of 13 %, increasing the average bleaching for this duration. It is possible that the disc was accidentally exposed to direct fluorescent light during the experiment's setup. Excluding this disc, after 10 min of bleaching within the black bottles, the signal was bleached by 5 %. In contrast, in full daylight, the OSL signal of the quartz grains is reduced to less than 5 % after 5 s. It is important to note that while in the bleaching experiment, the black bottles were left open for the entire experiment time, during the HF etching procedure, the cap is removed only for a few seconds. Also, during the experiment, all the fluorescent lights in the laboratory were turned on, while during the procedure, we turn off the lights near the fume hood. Therefore, there is no risk of bleaching during this protocol.

4. Summary

We described a protocol that avoids the most risky factors of using HF in luminescence dating: working in the dark and pouring HF into open beakers. Any lab that had a beaker accidentally turned over would appreciate it. It is also light-safe and avoids any access exposure of the samples to laboratory light. This protocol was devised over 22 years ago and has since been used 10 – 15 times yearly. Not a single accident with HF body exposure happened during that time. This protocol is also economical regarding HF; only 15 mL are used per sample. We deem this protocol as very safe and encourage other laboratories to adopt it or a variation of it.

Appendix: HF etching protocol

Equipment list:

1. Samples (18 in the case of the GSI)
2. Labeled black, opaque polyethylene bottles with caps, one for each sample; 1 cap has two holes for the tube and air.
3. Suction tube with stopping restrains, about 60 cm long
4. Peristaltic pump, calibrated (calibrated pumping rate at the GSI is 10 mL per minute)
5. Concentrated HF acid (40%) bottle with a narrow opening (Fig. 1a)
6. Any plastic bottle (250-500 mL) with a tight screw cap to collect the spent HF, to be later disposed with other chemical waste.
7. Timer
8. Watch with minutes

Procedure

In the dark lab:

- Weigh about 3 g sample into a bottle and close with the cap.
- If there is less than 3 g of quartz, mark the weight on the label.
- Repeat for all samples.

In a lit lab in a fume hood (procedure video is available at https://youtu.be/lZbMpKDgf-s):

- Put on safety gear.
- Turn off fluorescent lights near the fume hood but leave other lights on for comfortable vision; turn on ventilation in the fume hood.
- Set up the peristaltic pump. Put one end of the tube into the HF bottle and the other into the black sample bottle lid with the holes.
- Turn on the pump and turn on the timer, wait the designated time (marked by the timer), and turn the pump off (for the first sample, start the timer only when the acid reaches the sample bottle).
- The pierced lid with the tube will now be passed to the following sample, while at the same time, a normal lid will be placed on the sample that has just received HF. Partially close the lid on the first sample to allow for any gasses to be emitted and, at the same time, prevent unnecessary exposure to light. Exchange lids as quickly as possible.
- Repeat for all samples. From time to time, twirl the waiting bottles. In the last sample, take the tube out of the HF bottle after a minute and let the tube empty into the black bottle.

After 40 minutes of introducing HF to the first sample:

- Open the first sample and carefully drain most of the spent HF into the waste bottle. The grains will collect in the bottle's shoulder. Add 200 mL water, close, and set aside. After the following sample is drained and filled with water, return to the first sample, slowly pour most of the water into the sink while the water is running, and refill with ~200 mL water. Close the bottle tightly and place it away. Your first sample is done.
- Continue with the next bottle. Note that one rinse takes place right after draining the HF, the second a few minutes later, after the following sample has been drained. That leaves time for the grains to settle.
- If there is a very little sample (less than 0.5 g), leave it in HF for only 20 minutes so that not all is dissolved, and be extra slow and careful when pouring out and rinsing.
- Now the samples are ready to be returned to the dark lab for additional rinsing and following quartz extraction steps.

References

Aitken, M. J. *Thermoluminescence dating*. Studies in archaeological science. Academic Press, 1985.

Bell, W. T. and Zimmerman, D. W. *The effect of HF acid etching on the morphology of quartz inclusions for thermoluminescence dating*. Archaeometry, 20: 63–65, 1978.

Bertolini, J. C. *Hydrofluoric acid: a review of toxicity*. The Journal of emergency medicine, 10: 163–168, 1992.

Duval, M., Guilarte, V., Campa na, I., Arnold, L., Miguens, L., Iglesias, J., and González-Sierra, S. *Quantifying hydrofluoric acid etching of quartz and feldspar coarse grains based on weight loss estimates: implication for ESR and luminescence dating studies.* Ancient TL, 36: 1–14, 2018.

Faershtein, G., Porat, N., Avni, Y., and Matmon, A. *Aggradation–incision transition in arid environments at the end of the Pleistocene: an example from the Negev Highlands, southern Israel*. Geomorphology, 253: 289–304, 2016.

Muriale, L., Lee, E., Genovese, J., and Trend, S. *Fatality due to acute fluoride poisoning following dermal contact with hydrofluoric acid in a palynology laboratory*. The Annals of occupational hygiene, 40: 705–710, 1996.

Murray, A., Buylaert, J. P., and Thiel, C. *A luminescence dating intercomparison based on a Danish beach-ridge sand*. Radiation Measurements, 81: 32–38, 2015.

Porat, N., Faerstein, G., Medialdea, A., and Murray, A. S. *Re-examination of common extraction and purification methods of quartz and feldspar for luminescence dating*. Ancient TL, 33: 22–30, 2015.

Wang, X., Zhang, Y., Ni, L., You, C., Ye, C., Jiang, R., Liu, J., and Han, C. *A review of treatment strategies for hydrofluoric acid burns: current status and future prospects*. Burns, 40: 1447–1457, 2014.

Wintle, A. G. *Luminescence dating: Laboratory procedures and protocols*. Radiation Measurements, 27: 769–817, 1997.

Reviewers

Michel Lamothe

Ancient TL

The LF02 automated luminescence reader

Luis Baly[1*], Raul Arteche[1], Piet van Espen[2], Jossué Arteche[1], Inés Quesada[1], María García[1], Hector Lubián[1], Teresita Cepero[1], Marie Baly[1], Juan Carlos Gutiérrez[1], Armando Chávez[1], Roberto A.D. Valle[3] and Leandro P. Hernández[3]

[1] Centro Aplicaciones Tecnológicas y Desarrollo Nuclear (CEADEN). Calle 30 No 502, Playa, La Habana, Cuba, AP 6122
[2] Department of Chemistry, University of Antwerp, Middelheimcampus G.V.130 Groenenborgerlaan 171 2020, Antwerp, Belgium
[3] Instituto de Geología y Paleontología- Servicio Geológico de Cuba (IGP). Vía Blanca 1001, San Miguel del Padrón, La Habana, Cuba

[*]Corresponding Author: baly@ceaden.edu.cu

Received: November 6, 2023; in final form: December 16, 2023

Abstract

In the present work the LF02 automated luminescence reader is introduced. The construction of the LF02 is part of a project aimed at creating capacities to support the activities of the luminescence dating laboratory at CEADEN in terms of carrying out sediment dating and basic research on quartz luminescence. To accomplish this task, a robust design with a basic structure capable of executing long measuring sequences was proposed. Along with the description of the reader, design concepts aimed at reducing the measurement time are analyzed in detail. To evaluate the effect of each design idea, the term reader productivity is defined. For the evaluation of the LF02 productivity, two different cases are analyzed. In the first one, the sample dose to recover is equivalent to 151 s of beta irradiation, while in the second case the time of irradiation is 833 s. The results show that the introduction of these ideas produces a significant reduction of time needed for completing a SAR sequence.

Keywords: luminescence dating, automated reader, quartz

1. Introduction

After the pioneering work by Huntley et al. (1985) proposing the optical dating of sediments and the subsequent standardization of this method through the development of the single aliquot regenerative dose (SAR) protocol (Murray & Wintle, 2000), optically stimulated luminescence (OSL) has become the major dating tool in Quaternary geology, at least for the past 100 000 years (Wintle, 2008). There is no doubt that the development and commercialization of automated luminescence readers, specifically designed for this application (Bøtter-Jensen et al., 2000; Bortolot, 2000; Richter et al., 2013), has played an important role in the dissemination of this technique. Single grain measurements based on laser stimulation (Duller et al., 1999; Bøtter-Jensen et al., 2003), new more powerful stimulation systems including violet excitation wavelengths (Jain, 2009; Lapp et al., 2015), pulsed excitation-detection systems for time resolved OSL measurements (Denby et al., 2006), EM-CCD detection systems (Kook et al., 2015) and the introduction of small X-ray irradiation sources (Thomsen et al., 2006) are some examples of the new capabilities added in recent years to these instruments.

In Cuba, the correct description and interpretation of the Quaternary geology requires the establishment of the absolute ages of rocks and sedimentary deposits. Also, the development of policies to reduce the impact of sea level rise on the Cuban territory requires the assessment of recent tectonic movement in coastal areas. In both cases, OSL dating is a valuable technique. This explains the interest in creating national capabilities to carry out sediment dating studies

Figure 1. View of the LF02 automated reader

using the OSL technique.

While most of the equipment employed in dating laboratories can also be used in other scientific laboratories, the automated OSL readers are more specific, which makes them expensive and difficult to maintain. Also, for some countries the access to this instrument is limited by export restrictions associated with the radioactive source incorporated into them. Therefore, the development of an automated reader was one of the goals of the project for the creation of the luminescence dating laboratory at CEADEN.

The present paper describes the LF02 automated luminescence reader, routinely used at the CEADEN dating laboratory. Due to the initial projection that only a single reader would be available, the reduction of the measuring time guided the conception and design stages. Therefore, along with the description of the reader, the design concepts aimed at reducing the measurement time are analyzed in detail.

2. Measuring time and reader productivity

In the present work, the measuring time is defined as the time needed to complete a sequence based on the SAR protocol (t_{SAR}). To propose solutions with a positive impact on the measuring time, a conceptual analysis of the dependence of t_{SAR} on the experimental variables becomes necessary. In general, t_{SAR} can be defined by the following equation:

$$t_{\mathrm{SAR}} = t_I + t_M \tag{1}$$

Here, t_I is the total time used for sample irradiation, while t_M represents the duration of all the processes linked to the luminescence measurement such as preheating, OSL measurement or illumination. Both, t_I and t_M, include the time spent on sample positioning.

In Equation 1 it is assumed that at any moment, just one process, irradiation or measurement, is taking place. In the case when irradiation and luminescence measurement are occurring simultaneously, t_{SAR} needs to be represented differently:

$$t_{\mathrm{SAR}} = t_I + (1-b) \cdot t_M \tag{2}$$

Here b is a parameter describing the time overlapping between both processes, and its value ranges from 0 (no overlapping) up to 1 (full overlapping). Equation 2, as a more general case, reveals the pathways to reduce t_{SAR}. The first approach would be the reduction of t_I or t_M; the second one would be the execution of the sequence in a way that measurement and irradiation are run simultaneously.

t_{SAR} depends on several factors such as the number of aliquots, the number of points used to construct the dose response curve, the equivalent dose of the sample and the dose rate of the beta source. Therefore, the use of t_{SAR} to evaluate the reduction of the measuring time has practical value only when the experimental parameters are fixed. Thus, it would be useful to have an indicator of the reader time performance, even when the experimental conditions are different. With such a purpose the term reader productivity (Pr) is proposed. Pr is defined by the following expression:

$$Pr = \frac{D_{\mathrm{e}} \cdot N_L \cdot N_a}{t_{\mathrm{SAR}} \cdot \dot{D}_\beta} \tag{3}$$

Here $\mathrm{D_e}$ is the sample equivalent dose (Gy) (previously

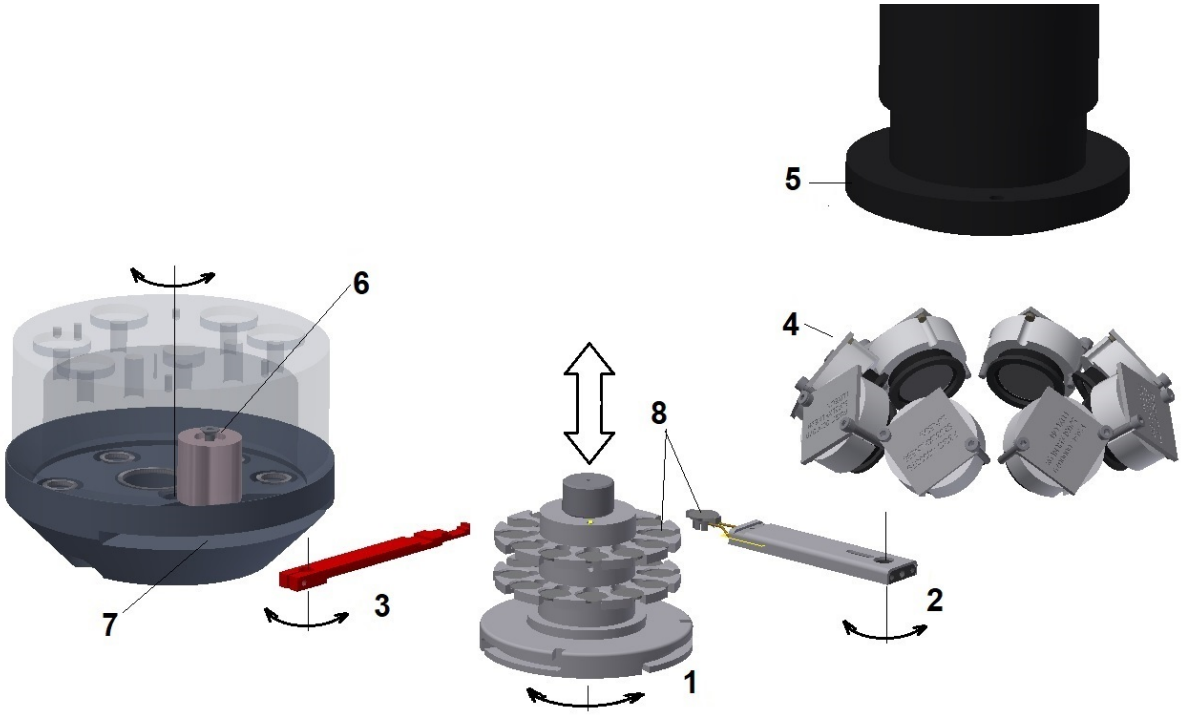

Figure 2. The schematic representation of the of the LF02 measuring chamber. The axes and arrows show the displacement of the moving elements. 1 - sample holder, 2 - measuring arm, 3 - irradiation arm, 4 - LEDs, 5 - PMT, 6 - beta source, 7 - slit for sample entry into the irradiator, 8 - sample disc.

known or measured after running the SAR sequence); N_L is the number of data types in the sequence; N_a is the number of aliquots, $\dot{D}_\beta$ is dose rate (Gy/s) of the beta source and t_{SAR} (s) is the time the reader needed to complete the SAR sequence. Even when this definition may not consider all the situations, it describes the reader time performance: the higher the value of Pr the better the reader time performance.

3. The LF02 automated reader

The LF02 (Fig. 1) follows the basic structure of this sort of instrument: A beta irradiation source (on the left) used for in-situ irradiation, a stimulation detection system (on the right) based on an array of LEDs, a photomultiplier working in the photon counting regime, and the automated sample positioning system holding up to 24 samples. The reader, which is controlled from a computer, has also supporting electronics with its associated software. The measuring chamber of the LF02 was designed to support vacuum. Vacuum conditions are expected to be needed for the future development of optically stimulated electron (OSE) measurement capabilities(Ankjærgaard et al., 2009).

Two mechanical arms pick up sample discs from the holder and place them in the beta irradiator or in the stimulation-detection unit, allowing that any sample can be irradiated while any other is being measured (Fig. 2). A short presentation showing the sample positioning system in action can be found at https://www.youtube.com/watch?v=_znlq6wXB94. The arm taking samples to the stimulation-detection unit includes a Kanthal resistive heater that reaches 500 °C with a maximum heating rate of 20 °C/s. The heating rate and temperature stabilization is realized through a tuned digital PID control system with a 2 °C maximal error.

The optical stimulation system comprises 8 ports for installing LEDs. Four of them are used for 1W blue LEDs with focusing optics ($\lambda =$ 470 nm, $P_T =$ 200 mW in the sample zone); two for IR LEDs with focusing optics ($\lambda =$ 850 nm, $P_T =$ 150 mW in the sample zone), and the other two are auxiliary ports for a wide range of applications, including another set of LEDs with different wavelength emission. Each LED unit is controlled by a current feedback stabilization system. During the design of the stimulation unit, special care was taken to produce a homogeneous illumination pattern at the sample position (Quesada et al., 2004).

For luminescence detection, the LF02 uses a 9235QB photomultiplier. The quartz OSL is filtered with 7 mm of ultraviolet glass filter UFC6 with a maximum transmittance at 360 nm, comparable to the commonly used U340 filter.

A $^{90}Sr/^{90}Y$ beta source, used for in-situ irradiation, provides a dose rate of 0.033 $\pm$ 0.002 Gy/s. For irradiation, the sample disc is introduced inside the irradiator shielding through a small slit (Fig. 2). Once the sample is in the irradiation position, the radioactive source, which is mounted in a horizontal rotating cylinder, is turned 180° from its parking position to the irradiation port. To irradiate highly sensitive luminescence detectors, such as Al_2O_3:C (Akselrod

Figure 3. The sample holder, hosting up to 24 discs (below), and the container.

et al., 1990), a low dose rate (0.5 μGy/s) Bremsstrahlung (X-Rays) irradiation mode was implemented (Burbidge & Duller, 2003). This method differs from the beta irradiation mode in that during the irradiation the source remains at the parking position.

The sample holder has two sections (upper and lower), each one holding up to 12 samples. The sample holder is assembled with a light-tight container (Fig. 3), to keep the samples in the dark. Once the container with the sample holder is coupled to the reader, the sample positioning system disengages the sample holder from the container and introduces it into the measuring chamber without exposing to the light. Taking advantage of this feature, the LF02 is installed in a room with no red-light illumination system.

The electronics of the LF02 is designed to resolve the simultaneous control of irradiation, sample positioning, sample heating, luminescence measurement and data transmission. The electronic core of the LF02 uses the FPGA technology. Measuring modes such as TL, CW-OSL, LM-OSL and POSL are implemented with a maximum time resolution of 500 ns per channel and 32 bits / 120 MHz counting system.

The measuring sequences for the LF02 are generated with an application called *GenSec*. *GenSec* is a home-made application and generates a perfectly readable xml-format file with an .slf extension. The sequence file includes general information, the measuring parameters and the status of each process, indicating if the process is pending, running or done. An example of the sequence file can be found in the Supplementary Material.

To run the sequence, the defined sequence file is loaded by another application called *GenExe*, which communicates with the reader and controls the execution of the sequence. In the LF02, the input and output files have the same format. As the measuring process goes, the status of each process is updated and the results of the measurement and the time of measurement are appended to the sequence file for subsequent analysis. This allows sequence pausing, and resuming later from the first pending process.

4. Methods for t_{SAR} reduction

In this section the methods implemented in the LF02 reader to reduce t_{SAR} are explained. The methods are presented according to their impact on the time reduction starting from the one with least impact.

a) ***Increasing the optical stimulation power***. Assuming that the OSL curve is described by a single exponential decay $I(t) = I_0 e^{-\sigma(\lambda) P_{\mathrm{LED}} t}$, where $\sigma(\lambda)$ is the photoionization cross-section and P_{LED} is the intensity of the optical stimulation radiation (Kuhns et al., 2000), then the higher the value of P_{LED} the faster the decay. Presently available blue LEDs with enhanced optical power allow the construction of optical stimulation units with stimulation power at the sample position exceeding 200 mW/cm^2. Figure 4 shows the OSL curve measured in the LF02 reader with 90% of the maximal optical power of a fast component dominated quartz irradiated to 5 Gy. As it is observed, only 10 seconds are needed to measure the whole decay curve.

b) ***Merging processes during OSL measurements***. Each cycle of the SAR protocol comprises a group of processes such as preheating and OSL measurement, sequentially executed one after another in the stimulation-detection unit. When these processes are executed individually, after finishing each process the sample disc is returned back to the sample holder following a cooling down process. The merging concept implements two ideas: firstly, samples are not sent back to the sample holder until the last

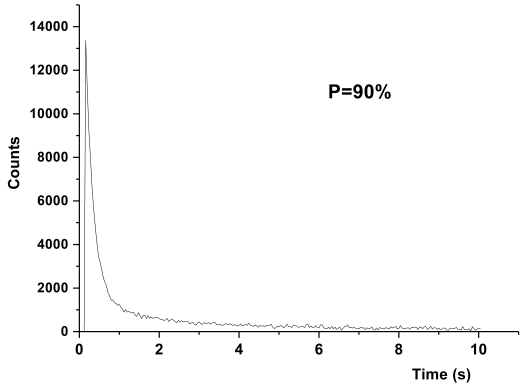

Figure 4. OSL curve for the 5 Gy reference quartz material.

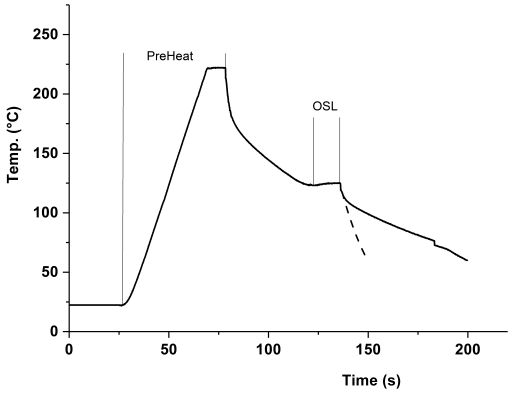

Figure 5. The continuous temperature profile of the merged preheating and OSL measurement processes. The dashed curve shows the effect of the gas jet fast cooling on the profile.

process of the group is executed; and secondly, the sample is heated with a continuous temperature cycle, and only when the last process in the group is executed, the sample is cooled down to the safe temperature. With these ideas, the time used in sample positioning and in cooling down the sample is reduced. Figure 5 shows the temperature profile of a merged pre-heating and OSL measurement. After linear pre-heating to 220 °C, and keeping that temperature for 10 s, the sample is not returned to the sample holder; the system waits for the natural decrease of sample temperature to 125 °C and following a temperature stabilization, the OSL curve is measured for 10 s. Then the sample is cooled down to a safe temperature (60 °C) after which the sample is sent back to the holder. The merging of the OSL measuring processes is defined during the sequence edition. After defining individual processes, the processes to be merged are selected and the command "MERGE" is applied.

c) ***Fast cooling***. Before the sample is returned to the sample holder the system waits until the sample cools down to a safe temperature of 60 °C. If the cooling process is based on the natural heat exchange, depending on the sample temperature it may take 1 – 2 minutes before the safe temperature is reached. To reduce this time, in the LF02 a gas jet nozzle located beneath the heater is used to rapidly cool down the sample at the end of the heating profile. With this system, the cooling down process from 125 °C is reduced from 1 minute to less than 20 seconds (Fig. 5).

d) ***Two-queues scheme***. In the LF02 reader, a sequence can be executed using three different schemes. The first one is the "first sample first" (FSF) scheme, in which all the processes of the first sample are executed first; and then all the processes of the second sample, and so on. The second scheme is the "first process first" (FPF) scheme, in which the "first process" of all the samples is executed first and then the "second process" of all the samples and so on. The third scheme, which is based on the possibility of independently moving samples to irradiation or to the measuring unit, is called "two-queues" (2Q). In the 2Q scheme both types of processes, irradiation and measurement, are run simultaneously. As soon as the system detects that either the irradiation source or the measuring system is available, it looks for a sample, whose first pending process matches the type of the available port and executes it. Using this scheme, due to the time overlapping of the irradiation and measuring processes, a reduction of the overall measuring time is produced.

e) ***External irradiation***. As it was explained above, the sample container of the LF02 allows the transport of the sample discs without exposing them to light. In addition to this, the small sizes and the thin walls of this aluminum container make possible the simultaneous irradiation of all the samples by irradiating the container in a gamma irradiation facility, avoiding sample disc manipulation. For old samples requiring long times of beta irradiation the external irradiation is a convenient method to reduce the irradiation time when all the samples are expected to receive the same dose. The external irradiation is defined during the sequence edition as an independent process. When the LF02 finds an external irradiation process the sequence advances until all the samples are waiting for the external irradiation. After this point the reader automatically sends the sample holder to the container and advises the operator of an awaiting external irradiation. The external irradiation can reduce the overall irradiation time of a single dose point from several hours to some minutes. Due to the relatively high dose rate of gamma irradiation facilities, the external irradiation is not suitable for young samples.

5. Materials and methods

A previously sensitized quartz material with diameters between 180 and 250 μm and showing a predominant fast component in the OSL signal was used to prepare two samples. The first sample is an internal reference material gamma irradiated in a ^{60}Co secondary calibration facility to 5.0 ± 0.1 Gy. The other sample was irradiated in a gamma irradiation facility at CEADEN for 300 s. The dose received by this sample was measured in the LF02 reader using a standard SAR protocol resulting in a dose of 27.5 ± 1.6 Gy. For these two samples a 6 mm diameter spot of quartz grains was mounted on a stainless steel discs.

The reference conditions for the SAR protocol were: Preheat temperature, 220 °C at 5 °C/s for 10 s; cut heat 200 °C at 5 °C/s for 5 s; optical power = 25%; OSL measuring time 40 s and test dose of 30 s. The preheat temperature was determined from a preheat plateau test. When using increased optical power (90 %), the conditions are the same except the OSL curve was measured during 10 s. Using the reference conditions, the beta dose rate was found to be

Procedure designation	Procedure description	t_{SAR} (hours)	Time reduction (%)	*Pr*	D_e(Gy)
A0	5 Gy sample, P_{LED}=20%, no merging, no fast cooling, FPF mode	23	-	0.26	5.0 ± 0.2
A1	5 Gy sample, P_{LED} =20%, no process merging, fast cooling, FPF mode	16	31	0.37	5.1 ± 0.1
A2	5 Gy sample, P_{LED} =90%, process merging, fast cooling, FPF mode	12.5	45	0.48	5.1 ± 0.2
A2-2Q	5 Gy sample, P_{LED} =90%, process merging, fast cooling, 2Q mode	10	56	0.60	4.8 ± 0.2
A2-2Q-HD	27.5 Gy sample, P_{LED} =90%, process merging, fast cooling, 2Q mode	16.3	-	2.24	27.5 ± 1.6
A2-2Q-EXT	27.5 Gy sample, P_{LED} =90%, process merging, fast cooling, 2Q mode, external irradiation	10	38	3.66	26 ± 2.4

Table 1. Comparison of the time needed to complete a SAR sequence (t_{SAR}) and reader productivity (*Pr*) using different procedures. The time reduction is calculated using procedures A0 and A2-2Q-HD as reference for the 5 Gy and 27.5 Gy samples respectively. The equivalent dose (D_e) obtained for each procedure is also presented.

0.033 ± 0.001 Gy/s. At this dose rate, the 5 and 27.5 Gy doses are produced after 151 and 833 s of irradiation respectively.

A ^{60}Co gamma irradiation facility was used for external irradiation. With the purpose of homogenizing the dose, during the external irradiation the container is mounted in a spinning system. To achieve irradiation uniformity better than 4% only the upper section of the sample holder was used (12 samples). Considering the beta dose rate as a reference value, the dose rate of the irradiation facility at the time of this experiment was 0.090 ± .006 Gy/s (324 ± 22 Gy/h), which is 2.7 times higher than the beta source dose rate. The overall transient dose appearing during the introduction and extraction of the container was 1.02 ± 0.05 Gy.

The value of t_{SAR} is defined as the time for completing a sequence of SAR protocol on 12 aliquots. Beside of the initial dose measurement (L_0) , the OSL response for three dose points (L_1, L_2, L_3) was used for the construction of the dose response curve. Two additional measurements were used for recuperation (L_4) and recycling (L_5) tests. A constant test dose of 30 seconds irradiation was given after the measurement of each dose point; and the corresponding OSL response (T_0 trough T_5) was measured. For the 5-Gy sample, the dose points were 100, 150 and 250 s of beta irradiation; for the 27.5 Gy sample, the dose points were 700, 850 and 1000 s of beta irradiation and when the gamma irradiation facility was used, the irradiation times were 270, 300 and 400 s. In the last case additional 20 minutes per irradiation point were employed for sample transferring and preparative works.

For both samples a linear regression was used to construct the dose response curve. For the 5 Gy sample the regression coefficient was better than 0.99; for the 27.5 Gy sample the regression coefficient was lower, 0.98, due to non-linear behavior of the dose response curve in that region. The criteria for aliquot acceptance were 1.00 ± 0.05 for the recycling ratio and 0.00 ± 0.05 for the recuperation. Among the 72 aliquots used in this study only 2 were rejected.

6. Results

Six different procedures were used to evaluate the proposed methods of time reduction. The procedures use different combinations of the methods proposed above. Table 1 shows the designation and the description of each procedure. The procedure denoted as A0 uses the reference conditions for the SAR protocol described in the previous section and it is executed with FPF scheme. The A1 procedure uses the same conditions as the A0 but the fast cooling method is added at the end of each heating profile. The A2 procedure combines increased stimulation power (90%), merging of processes during OSL measurement and fast cooling. Both A1 and A2 procedures are executed with FPF scheme. The A2-2Q procedure uses the same conditions as A2 but instead of using FPF scheme uses the 2Q scheme of sequence execution. All these procedures were tested with the 5 Gy sample.

For the 27.5 Gy sample the reference procedure is the A2-

2Q-HD. This procedure uses the same time reduction methods used in the A2-2Q procedure, and is denoted differently to mark the measurement of a sample with higher equivalent dose. The A2-2Q-EXT procedure uses the same conditions as A2-2Q-HD, with the difference that the dose points of L1, L2, L3 and L5 are given externally while test doses are given with the beta source. The results are presented in Table 1.

When comparing the procedures used in the 5-Gy sample, it is observed that the application of each method produces a reduction of the 23 hours needed for completing the reference procedure A0. In this sequence, the total irradiation time is 3.2 hours; which indicates that most of the time is dedicated to luminescence measurement.

The fast cooling introduced in the A1 procedure drastically reduces t_{SAR}. The reason of this significant time reduction is due to the reduction of time needed to cool down to the safe temperature, especially after preheating to 220 °C. The incorporation of other methods in A2 and A2-2Q procedures, allows decreasing the measuring time to less than half the time used in the reference method A0. When using *Pr* to analyze reader time performance, an increment of its value is observed as new methods of time reduction are added

In the case of the A2-2Q-HD procedure, the time needed to deliver a beta dose point is several times longer than the time spent in executing the group of processes to measure a single OSL signal; therefore, an almost complete time overlapping should be expected. For this procedure, the value of t_{SAR} (16.3 hours) is close to the total irradiation time (13.8 hours); indicating that the luminescence measuring process occurs behind the irradiation. Although the total irradiation time of the A2-2Q-HD procedure is 4.3 times greater than the one of A2-2Q, the corresponding ratio for t_{SAR} is less than 2. This is explained because in the low dose case, the time overlap is very low and very often the sequence gets blocked waiting for a luminescence measurement process to be finished. Finally, the application of the external irradiation method reduces the measuring time by nearly 40%, however this time reduction is principally due to the reduction of the irradiation time.

The evaluation of *Pr* for all procedures is also shown in Table 1. It can be observed that, as new methods of time reduction are applied, the reader productivity increases. A significant increment is found after the application of the fast cooling method. Another important increment is observed from the A2-2Q procedure to the A2-2Q-HD; confirming the previous conclusion that the 2Q scheme is more effective when beta irradiation times are longer than the typical 3-4 minutes duration of the luminescence measuring process (see Fig. 5). As expected, the higher *Pr* is obtained for the A2-2Q-EXT procedure in which all the proposed methods are combined.

The methods used here to reduce t_{SAR} change the conditions under which the equivalent dose is normally measured: higher photon counting rates, continuous heating profile, fast sample cooling, etc. Therefore it is important to check that these modifications do not produce significant variations in the measured equivalent dose. The results of this study are presented in Table 1. In the case of the 5-Gy sample, the results show that there is good agreement between the procedures and that all the procedures give a result close to the expected dose.

From the point of view of measuring conditions, there is almost no difference between A2-2Q and A2-2Q-HD procedures, except a higher photon counting rate during the OSL measurement in the A2-2Q-HD procedure. Nevertheless, for the 27.5 Gy sample used in this procedure, the photon counting rate is quite below the maximal counting rate of the detection system. Therefore, the accuracy of the 27.5 Gy dose obtained with the A1-2Q-HD method can be inferred from the correctness of the A1-2Q method, previously established. The comparison of the results given by A1-2Q-HD and A1-2Q-EXT methods shows good agreement, noticing a higher dispersion for the A1-2Q-EXT method; mainly motivated by the operator intervention during the gamma irradiation process.

7. Conclusions

The LF02 automated luminescence reader, routinely used at the CEADEN dating laboratory, has been described. Five methods proposed to reduce the time spent on equivalent dose measurements using the SAR protocol were evaluated. Three of these methods are related to the reduction of the luminescence measuring time, one related to the reduction of the irradiation time and the other oriented to produce time overlapping of irradiation and measurement. The application of these methods allowed a time reduction to less than half of the time without the implementation of the methods. The proposed *Pr* parameter proved useful for evaluating the reader productivity under different conditions. Based on the increment of *Pr*, the application of all these methods improved the reader time performance.

Acknowledgements

The authors want to thank Dr. Kristina J. Thomsen for the reviewing of a previous version of the manuscript and for the useful comments that significantly improved the paper. We also want to thank Rene Corremans and Jan Huysmans† for their remarkable contribution in the construction of the LF02.

References

Akselrod, M. S., Kortov, V. S., Kravetsky, D. J., and Gotlib, V. I. *Highly sensitive thermoluminescent anion-defective Al2O3 : C single crystal detectors*. Radiation Protection Dosimetry, 32: 15–20, 1990.

Ankjærgaard, C., Murray, A. S., Denby, P. M., and Jain, M. *Using optically stimulated electrons from quartz for the estimation of natural doses*. Radiation Measurements, 44: 232–238, 2009.

Bortolot, V. J. *A new modular high capacity OSL reader system*. Radiation Measurements, 32(5-6): 751–757, 2000.

Bøtter-Jensen, L., Bulur, E., Duller, G. A. T., and Murray, A. S. *Advances in luminescence instrument systems*. Radiation Measurements, 32(5-6): 523–528, 2000.

Bøtter-Jensen, L., Andersen, C. E., Duller, G. A. T., and Murray, A. S. *Developments in radiation, stimulation and observation facilities in luminescence measurements*. Radiation Measurements, 37(4): 535–541, 2003.

Burbidge, C. I. and Duller, G. A. T. *Combined gamma and beta dosimetry, using Al2O3 :C, for in situ measurements on a sequence of archaeological deposits*. Radiation Measurements, 37: 285–291, 2003.

Denby, P. M., Bøtter-Jensen, L., Murray, A. S., Thomsen, K. J., and Moska, P. *Application of pulsed OSL to the separation of the luminescence components from a mixed quartz/feldspar sample*. Radiation Measurements, 41: 774–779, 2006.

Duller, G. A. T., Bøtter-Jensen, L., Murray, A. S., and Truscot, A. J. *Single grain laser luminescence (SGLL) measurements using a novel automated reader*. Nuclear Instruments and Methods in Physics Research. B, 155: 506–514, 1999.

Huntley, D. J., Godfrey-Smith, D. I., and Thewalt, M. L. W. *Optical dating of sediments*. Nature, 313: 105–7, 1985.

Jain, M. *Extending the dose range: Probing deep traps in quartz with 3.06 eV photons*. Radiation Measurements, 44(5-6): 445–452, 2009.

Kook, M. H., Lapp, T., Murray, A. S., Thomsen, K. J., and Jain, M. *A luminescence imaging system for the routine measurement of single-grain OSL dose distributions*. Radiation Measurements, 81: 171–177, 2015.

Kuhns, C. K., Agersnap Larsen, N., and McKeever, S. *Characteristics of LM-OSL from several different types of quartz*. Radiation Measurements, 32: 413–418, 2000.

Lapp, T., Kook, M., Murray, A. S., Thomsen, K. J., Buylaert, J.-P., and Jain, M. *A new luminescence detection and stimulation head for the Risø TL/OSL reader*. Radiation Measurements, 81: 178–184, 2015.

Murray, A. S. and Wintle, A. G. *Luminescence dating of quartz using an improved single-aliquot regenerative-dose protocol*. Radiation Measurements, 32: 57–73, 2000.

Quesada, I., Otazo, M. R., Baly, L., and Gonzalez, Y. *Design of a blue LED stimulation unit with a highly uniform illumination pattern*. Ancient TL, 22(2): 29–34, 2004.

Richter, D., Richter, A., and Dornich, K. *Lexsyg-a new system for luminescence research*. Geochronometria, 40(4): 220–228, 2013.

Thomsen, K. J., Bøtter-Jensen, L., Denby, P. M., and Murray, A. S. *Luminescence response to irradiation using mini X-ray generators*. Nuclear Instruments and Methods in Physics Research. B, 252: 267–275, 2006.

Wintle, A. G. *Fifty years of luminescence dating*. Archaeometry, 50(2): 2008, 2008.

Reviewer

David Sanderson

Thesis Abstracts

Index

Charlotte Francoz

Saltmarsh Resilience in a Changing Climate: Geomorphological and Biological Processes in Natural and Managed Salt Marshes in the North East of Scotland

August 2023

School of Geographical and Earth Sciences , College of Science and Engineering, University of Glasgow, Scotland

Degree: Ph.D.

Supervisors: Larissa Naylor, David Sanderson, James Hansom

Salt marshes are regarded as one of the world's most productive ecosystems due to the unique habitat they provide, which is essential to our ecological structure, and their ability to act as sinks for organic and inorganic sediment. Salt marshes have long attracted human settlement and exploitation due to their location along the coast, on the sheltered shores typical of estuaries and tidal inlets. The permanent loss of saltmarsh ecosystems is between 25 and 50 percent of their global historical coverage, and the decline continues globally. This is exacerbated by rising temperatures, sea level rise, and increasing storm intensity, which erode salt marshes. Since 1945, roughly 15 percent of saltmarsh area in the United Kingdom has been lost due to human intervention, primarily agricultural and industrial reclamation, and is now being exacerbated by coastal erosion and sea level rise. Saltmarsh formation and development are influenced by the interdependence of physical and biological processes, whereas vertical growth and saltmarsh stability are highly dependent on sediment supply and tidal range. However, the cumulative impact of human disturbance and sea level rise on the fundamental saltmarsh dynamics remains unclear and must be better understood at both the local and global scales.

This thesis aimed to improve understanding of the processes, mechanisms and patterns that 1) favour saltmarsh formation and development 2) enable saltmarsh capacity to recover from environment and anthropological disturbances 3) promote some of the regulating and supporting services salt marshes provide. My thesis has carried out a biogeomorphological appraisal of the first salt marsh managed realignment in Scotland since its breaching in 2003 in comparison with two adjacent natural salt marshes across different time scales. The study has employed a methodology to assess jointly managed/anthropogenically modified and natural salt marshes at different temporal scales. A set of managed and adjacent natural salt marshes within the same salt marsh system at Nigg Bay, NE Scotland provided a comparative case study of the links between sediment availability, vegetation presence and saltmarsh stability over time and space. Above ground changes in vegetation and sedimentation patterns were quantified over different timescales from short (annual) to longer (centennial) timescale using a combination of field measurements: sediment deposition, sedimentation plates and DEM time series in tandem with vegetation sampling. This multi-method approach has proven to be a powerful tool to analyse spatial distribution patterns of sediment accretion. Below ground physical and biological changes were explored using a combination of traditional sedimentary techniques and applying Luminescence to salt marsh, to gain knowledge on the possible mechanisms driving these changes. These results were used to assess the potential implications on the supporting and regulating benefits that salt marshes provide, as such contributing to saltmarsh blue carbon inventories for natural and managed realignment salt marsh in Scotland; and, on capacity of marshes to keep up with rising sea levels.

The cumulative results of my thesis work highlight that natural salt marshes have limited space to respond to environmental changes, which reduces their long-term resiliency. In terms of sea level rise, the marsh is responding due to the accommodation space provided by the managed realignment.

Furthermore, the study has developed a new application of Optically Stimulated Luminescence (OSL) that challenges the results of conventional techniques and allows exploration of modern sediment material registering the impacts of recent climate change. This work thus adds an important dataset to the Scottish context and more broadly to the growing literature on the ability for managed realignment sites to replicate natural saltmarsh functions and thus ecosystem services.

A PDF of this thesis can be downloaded from: http://theses.gla.ac.uk/id/eprint/83810

Chang Huang

Developments and Applications of Luminescence Dating in Earth Sciences

November 2023

Department of Earth Sciences, The University of Hong Kong, Hong Kong, China

Degree: Ph.D.
Supervisor: Sheng-Hua Li

This thesis aims to address fundamental questions about developments and applications in luminescence dating in the past, present, and future, including the age range, accuracy, and thermochronological studies.

To estimate the equivalent dose (D_e) of calcite, a single-aliquot regenerative-dose (SAR) protocol with low-temperature measurements is employed. It uses the isothermal thermoluminescence (ITL) signals measured at ~ 225 – 240 °C, where a D_e vs. ITL temperature (D_e-T) plateau is observed. These ITL signals correspond to the TL signals of the 280 °C TL peak. Notably, ITL signals at 230 – 235 °C saturate at ~ 4000 – 5000 Gy, which has the potential to date geological and archaeological samples spanning the entire Quaternary period. The absence of detectable anomalous fading of ITL signals suggests that the signal is free of fading. Dose recovery tests further confirm the suitability of the SAR-ITL protocol for D_e estimation.

The SAR-ITL protocol was then employed to study the thermochronological applications of limestone rocks in the middle of the Nujiang River, southeastern Tibetan Plateau. The results show that apparent D_e values of ITL_{230} signals increase with increasing heights, while apparent ages increase before approximately 400 ka (the apparent age) and then reach dynamic equilibrium stages. From the isochron plot of apparent D_e values against dose rates, the effect lifetimes of ITL signals were obtained, which constrains the applicable ranges of ITL signals from calcite. It is proposed that calcite can be used in thermochronology within the applicable ranges from 530 $\pm$ 25 ka to the present.

The accurate luminescence dating of volcanic-related materials remains challenging. This study focuses on quartz minerals extracted from lava-baked sediments in the Tengchong volcanic field, southeastern the Tibetan Plateau, using the optically stimulated luminescence (OSL) technique. The results show that samples with initial OSL signals dominated by the fast component yield reliable ages. Conversely, samples dominated by unstable medium and slow components broadly underestimate their OSL ages, requiring corrections. By using the plot of D_e against recuperation for each aliquot, the underestimated OSL ages can be corrected. The final single-aliquot quartz OSL ages are consistent with single-grain quartz OSL and ^{14}C ages recording the same eruption event, thus validating the reliability of the dating ages.

The comprehensive research on photoluminescence (PL) emission spectra of various feldspar types remains poorly understood and the limited availability of instruments has hindered its research. This study investigated the PL properties of six feldspar types using a commercial Raman instrument. The results indicate that the number and medium positions of emission peaks depend on the specific feldspar types and samples analyzed. Additionally, the sensitivity of PL signals to irradiation dose varies across feldspar types and peak positions. Notably, PL emissions from ~ 865 and ~ 910 nm of K-feldspar are sensitive and show potential applicability for dating applications. The dose-response curves obtained using 860 – 870 nm PL signals of potassium feldspar conform to a relationship of a single saturating exponential function between the signal and irradiation dose. This study demonstrates that a commonly available Raman system can be utilized for PL measurements of single grains.

Bibliography

Compiled by Sebastien Huot
From May 31, 2023 to December 1, 2023

Various geological applications

- aeolian

Buró, B., Négyesi, G., Varga, T., Sipos, G., Filyó, D., Jull, A.J.T., Molnár, M., 2022. Soil organic carbon dating of paleosoils of alluvial fans in a blown sand area (Nyírség, Hungary). Radiocarbon 64, 1-19, http://doi.org/10.1017/RDC.2022.5

Fernández-López de Pablo, J., Polo-Díaz, A., Ferrer-García, C., Poch, R.M., 2023. Heinrich Stadial 1 continental sand dunes and Middle to Late Holocene paleosol sequences in SE Iberia: Implications for human occupation and site formation processes. CATENA 232, 107447, http://doi.org/10.1016/j.catena.2023.107447

Forman, S.L., Wu, Z., Wiest, L., Marin, L., Mayhack, C., 2023. Late Quaternary fluvial and aeolian depositional environments for the western Red River, Southern Great Plains, USA. Quaternary Research 115, 3-24, http://doi.org/10.1017/qua.2023.15

Helm, C.W., Carr, A.S., Cawthra, H.C., De Vynck, J.C., Dixon, M.G., Gräbe, P.-J., Thesen, G.H.H., Venter, J.A., 2023. Tracking the extinct giant Cape zebra (Equus capensis) on the Cape south coast of South Africa. Quaternary Research 114, 178-190, http://doi.org/10.1017/qua.2023.1

Hu, G., Hu, J., Yu, L., Yang, L., Liu, X., Xiao, F., Dong, Z., 2023. Holocene aeolian activity triggered by climate change and endorheic-exorheic drainage transition in the Headwater Region of the Yellow River, Tibetan Plateau. Geomorphology 441, 108890, http://doi.org/10.1016/j.geomorph.2023.108890

Li, Y., Han, L., Li, X., 2024. Positive correlation between dust activity and humidity in arid Central Asia during the Holocene. Quaternary Science Reviews 324, 108442, http://doi.org/10.1016/j.quascirev.2023.108442

Liu, B., Zhao, H., Yang, F., Liang, A., Sun, A., Niu, Q., Li, S., 2023. A new aeolian activity proxy based on analysis of the grain size characteristics of surface soils across the Tengger Desert, northwest China, and its application to a Quaternary aeolian succession. Palaeogeography, Palaeoclimatology, Palaeoecology 622, 111594, http://doi.org/10.1016/j.palaeo.2023.111594

Mueller, D., Raith, K., Bretzke, K., Fülling, A., Parker, A.G., Parton, A., Preston, G.W., Jasim, S., Yousif, E., Preusser, F., 2023. Luminescence chronology of fluvial and aeolian deposits from the Emirate of Sharjah, UAE. Quaternary Research 112, 111-127, http://doi.org/10.1017/qua.2022.51

Song, H., Yang, X., Preusser, F., Fülling, A., Chen, B., 2023. Paleoenvironmental changes in the eastern Kumtag Desert, northwestern China since the late Pleistocene. Quaternary Research 116, 133-147, http://doi.org/10.1017/qua.2023.38

Sweeney, M.R., McDonald, E.V., Chabela, L.P., Hanson, P.R., 2020. The role of eolian-fluvial interactions and dune dams in landscape change, late Pleistocene–Holocene, Mojave Desert, USA. GSA Bulletin 132, 2318-2332, http://doi.org/10.1130/B35434.1

Woywitka, R., Froese, D., Lamothe, M., Wolfe, S., 2022. Late Pleistocene aeolian deposition and human occupation on the eastern edge of the deglacial corridor, northeastern Alberta, Canada. Quaternary Research 110, 100-113, http://doi.org/10.1017/qua.2022.14

- cave

Fusco, D.A., Arnold, L.J., Gully, G.A., Levchenko, V.A., Jacobsen, G.E., Prideaux, G.J., 2023. Revisiting the late Quaternary fossiliferous infills of Cathedral Cave, Wellington Caves (central eastern New South Wales, Australia). Journal of Quaternary Science 38, 505-525, http://doi.org/10.1002/jqs.3497

Hu, Y., Zhang, J., Lu, H., Hou, Y., Huang, W., Li, B., 2023. New chronology of the deposits from the inner chambers of the Guanyindong cave, southwestern China. Journal of Archaeological Science 159, 105872, http://doi.org/10.1016/j.jas.2023.105872

Pawełczyk, F., Bolik, A., Błachut, B., Kamińska, A., Opała-Owczarek, M., Malik, I., Wojcik, M., Zakrzewska, Z., Pawlak, Z., Poręba, G., 2023. Development of chronology for historical mining shaft remains in the vicinity of Tarnowskie Góry based on radiocarbon, luminescence and dendrochronological dating. Geochronometria 50, 81-90, http://doi.org/10.2478/geochr-2023-0004

- coastal

An, Y., Feng, X., Liu, J., Saito, Y., Qiu, J., Zhang, X., Wang, H., Chen, L., 2023. Development of a Middle–Late Holocene subaqueous clinoform in the northern Jiangsu coastal zone, western South Yellow Sea. Geomorphology 439, 108853, http://doi.org/10.1016/j.geomorph.2023.108853

Arce Chamorro, C., Vidal Romaní, J.R., Grandal d'Anglade, A., Sanjurjo Sánchez, J., 2023. Aeolization on the Atlantic coast of Galicia (NW Spain) from the end of the last glacial period to the present day: Chronology, origin and evolution of coastal dunes linked to sea-level oscillations. Earth Surface Processes and Landforms 48, 198-214, http://doi.org/10.1002/esp.5481

Boyd, S.L., Kinnaird, T.C., Srivastava, A., Whittaker, J.E., Bates, C.R., 2022. Investigation of coastal environmental change at Ruddons Point, Fife, SE Scotland. Scottish Journal of Geology 58, sjg2022-2005, http://doi.org/10.1144/sjg2022-005

Ellerton, D., Rittenour, T.M., Shulmeister, J., Roberts, A.P., Miot da Silva, G., Gontz, A., Hesp, P.A., Moss, P., Patton, N., Santini, T., Welsh, K., Zhao, X., 2022. Fraser Island (K'gari) and initiation of the Great Barrier Reef linked by Middle Pleistocene sea-level change. Nature Geoscience 15, 1017-1026, http://doi.org/10.1038/s41561-022-01062-6

Helm, C.W., Carr, A.S., Cawthra, H.C., De Vynck, J.C., Dixon, M.G., Lockley, M.G., Stear, W., Venter, J.A., 2023. Large Pleistocene tortoise tracks on the Cape south coast of South Africa. Quaternary Research 112, 93-110, http://doi.org/10.1017/qua.2022.50

Kluesner, J.W., Johnson, S.Y., Nishenko, S.P., Medri, E., Simms, A.R., Greene, H.G., Gray, H.J., Mahan, S.A., Padgett, J.S., Krolczyk, E.T., Brothers, D.S., Conrad, J.E., 2023. High-resolution geophysical and geochronological analysis of a relict shoreface deposit offshore central California: Implications for slip rate along the Hosgri fault. Geosphere 19, 1788-1811, http://doi.org/10.1130/GES02657.1

Leknettip, S., Chawchai, S., Choowong, M., Mueller, D., Fülling, A., Preusser, F., 2023. Sand ridges from the coastal zone of southern Thailand reflect late quaternary sea-level history and environmental conditions in Sundaland. Quaternary Science Reviews 316, 108264, http://doi.org/10.1016/j.quascirev.2023.108264

Neto de Carvalho, C., Belo, J., Figueiredo, S., Cunha, P.P., Muñiz, F., Belaústegui, Z., Cachão, M., Rodriguez-Vidal, J., Cáceres, L.M., Baucon, A., Murray, A.S., Buylaert, J.-P., Zhang, Y., Ferreira, C., Toscano, A., Gómez, P., Ramírez, S., Finlayson, G., Finlayson, S., Finlayson, C., 2023. Coastal raptors and raiders: New bird tracks in the Pleistocene of SW iberian Peninsula. Quaternary Science Reviews 313, 108185, http://doi.org/10.1016/j.quascirev.2023.108185

Oliver, T.S.N., Owers, C.J., Tamura, T., van Bracht, D., 2023. Holocene estuary infill leads to coastal barrier initiation from fluvial sand supply in southeastern Australia. The Holocene 33, 1489-1503, http://doi.org/10.1177/09596836231197744

Prasad, P., Loveson, V.J., Kumar, V., Shukla, A.D., Chandra, P., Verma, S., Yadav, R., Magotra, R., Tirodkar, G.M., 2023. Reconstruction of Holocene relative sea-level from beach ridges of the central west coast of India using GPR and OSL dating. Geomorphology 442, 108914, http://doi.org/10.1016/j.geomorph.2023.108914

Santos, N.B., Lavina, E.L.C., Paim, P.S.G., Tatumi, S.H., Yee, M., dos Santos, V.O., Kern, H.P., 2022. Relative sea level and wave energy changes recorded in a micro-tidal barrier in southern Brazil. Quaternary Research 110, 13-25, http://doi.org/10.1017/qua.2022.23

Sechi, D., Andreucci, S., Cocco, F., Pascucci, V., 2023. Stratigraphy and chronology of the Cala Mosca site, SW Sardinia (Italy). Quaternary Research 112, 160-179, http://doi.org/10.1017/qua.2022.45

Sydor, P., Uścinowicz, S., 2023. Driving forces and determinants of barrier coast evolution in the Holocene observed on the southern coast of the Baltic Sea. The Holocene 33, 759-780, http://doi.org/10.1177/09596836231163507

Ward, I., Healthy Country Program Team, T., Guilfoyle, D., O'Donnell, A., Byrne, C., Macphail, M., Hopper, S.D., 2023. Remnant peat deposit provides clues to the inundated cultural landscapes of Kepa Kurl, southwestern Australia. The Holocene 33, 671-684, http://doi.org/10.1177/09596836231157067

- earthquake (and fault related)

DuRoss, C.B., Briggs, R.W., Gold, R.D., Hatem, A.E., Elliott, A.J., Delano, J., Medina-Cascales, I., Gray, H.J., Mahan, S.A., Nicovich, S.R., Lifton, Z.M., Kleber, E., McDonald, G., Hiscock, A., Bunds, M., Reitman, N.G., 2022. How similar was the 1983 Mw 6.9 Borah Peak earthquake rupture to its surface-faulting predecessors along the northern Lost River fault zone (Idaho, USA)? GSA Bulletin 134, 2767-2789, http://doi.org/10.1130/B36144.1

Geçkin, B.Ş., Sözbilir, H., Özkaymak, Ç., Softa, M., Spencer, J.Q.G., Şahiner, E., Meriç, N., Deliormanlı, A.H., 2022. Evidence of surface rupture associated with historical earthquakes on the Gülbahçe Fault Zone (İzmir, Türkiye) and its application for determination of the surface fault-rupture hazard zone. Natural Hazards 114, 2189-2218, http://doi.org/10.1007/s11069-022-05467-9

Hu, G., Shao, Y., Liu, X., Zheng, W., Yao, Y., 2023. Paleoseismic evolution of the central section of the Serteng Shan fault at the northern Ordos Block (North China) since the Late Pleistocene. International Geology Review 65, 3272-3285, http://doi.org/10.1080/00206814.2023.2180778

Kelty, C., Onderdonk, N., 2022. Episodic Deformation and Topographic Development Along the Santa Ynez River Fault: A Blind Thrust in the Western Transverse Ranges of California. Tectonics 41, e2022TC007320, http://doi.org/10.1029/2022TC007320

Kluesner, J.W., Johnson, S.Y., Nishenko, S.P., Medri, E., Simms, A.R., Greene, H.G., Gray, H.J., Mahan, S.A., Padgett, J.S., Krolczyk, E.T., Brothers, D.S., Conrad, J.E., 2023. High-resolution geophysical and geochronological analysis of a relict shoreface deposit offshore central California: Implications for slip rate along the Hosgri fault. Geosphere 19, 1788-1811, http://doi.org/10.1130/GES02657.1

Liu, C.-R., Tian, Y.-Y., Ji, H., Ma, X., Wei, C.-Y., Dang, J.-X., Yin, G.-M., Zhou, Y.-S., Yuan, R.-M., 2023. Chronology analysis of huge landslide based on ESR dating materials on sliding face in carbonate areas of south eastern Tibet. Quaternary Geochronology 76, 101442, http://doi.org/10.1016/j.quageo.2023.101442

Luo, M., Chen, J., Owen, L.A., Qin, J., Yin, J., Yang, H., Liu, J., Gong, Z., Luo, J., 2022. A novel approach for reconstructing slip histories for bedrock fault scarps using rock surface luminescence dating. Geophysical Research Letters 49, e2022GL099526, http://doi.org/10.1029/2022GL099526

Müller, K., Polom, U., Winsemann, J., Steffen, H., Tsukamoto, S., Günther, T., Igel, J., Spies, T., Lege, T., Frechen, M., Franzke, H.-J., Brandes, C., 2020. Structural style and neotectonic activity along the Harz Boundary Fault, northern Germany: a multimethod approach integrating geophysics, outcrop data and numerical simulations. International Journal of Earth Sciences 109, 1811-1835, http://doi.org/10.1007/s00531-020-01874-0

Price, A.C., Woolery, E.W., Counts, R.C., Van Arsdale, R.B., Larsen, D., Mahan, S.A., Beck, E.G., 2019. Quaternary displacement on the Joiner Ridge Fault, Eastern Arkansas. Seismological Research Letters 90, 2250-2261, http://doi.org/10.1785/0220190149

Silva, P.G., Roquero, E., Medialdea, A., Bardají, T., Élez, J., Rodríguez-Pascua, M.A., 2022. Dating of Holocene Sedimentary and Paleosol Sequence within the Guadalentín Depression (Murcia, SE Spain): Paleoclimatic Implications and Paleoseismic Signals. Geosciences 12, http://doi.org/10.3390/geosciences12120459

- fluvial

Aksay, S., Schoorl, J.M., Versendaal, A., Wallinga, J., Maddy, D., van der Schriek, T., Demir, T., Aytaç, A.S., Veldkamp, A., 2024. Timing of gully development in a structurally controlled badland landscape, western Turkey. CATENA 234, 107616, http://doi.org/10.1016/j.catena.2023.107616

Bacon, S.N., Bullard, T.F., Kimball, V., Neudorf, C.M., Baker, S.A., 2023. Landscape response to hydroclimate variability shown by the post-Bonneville Flood (ca. 18 ka) fluvial-geomorphic history of the middle Snake River, Idaho, USA. Quaternary Research 113, 29-51, http://doi.org/10.1017/qua.2022.60

Bejarano-Arias, I., Van Wees, R.M.J., Alexanderson, H., Janočko, J., Perić, Z.M., 2023. Testing the applicability of quartz and feldspar for luminescence dating of pleistocene alluvial sediments in the Tatra Mountain foothills, Slovakia. Geochronometria 50, 50-80, http://doi.org/10.2478/geochr-2023-0002

Benito, G., Sanchez-Moya, Y., Medialdea, A., Barriendos, M., Calle, M., Rico, M., Sopeña, A., Machado, M.J., 2020. Extreme floods in small mediterranean catchments: Long-term response to climate variability and change. Water 12, http://doi.org/10.3390/w12041008

Benito-Calvo, A., Moreno, D., Fujioka, T., López, G.I., Martín-González, F., Martínez-Fernández, A., Hernando-Alonso, I., Karampaglidis, T., Bermúdez de Castro, J.M., Gutiérrez, F., 2022. Towards the steady state? A long-term river incision deceleration pattern during Pleistocene entrenchment (Upper Ebro River, Northern Spain). Global and Planetary Change 213, 103813, http://doi.org/10.1016/j.gloplacha.2022.103813

de Oliveira, M.A.T., Santos, J.C., Lemos, R., 2020. 80,000 years of geophysical stratigraphic record at the Serra da Capivara National Park, in northeastern Brazil: Uncovering hidden deposits and landforms at a canyon's floor. Journal of South American Earth Sciences 104, 102691, http://doi.org/10.1016/j.jsames.2020.102691

Delchiaro, M., Iacobucci, G., Della Seta, M., Gribenski, N., Piacentini, D., Ruscitto, V., Zocchi, M., Troiani, F., 2024. A fluvial record of late Quaternary climate changes and tectonic uplift along the Marche Piedmont Zone of the Apennines: New insights from the Tesino River (Italy). Geomorphology 445, 108971, http://doi.org/10.1016/j.geomorph.2023.108971

Devrani, R., Singh, V., Saini, H.S., Mujtaba, S.A.I., 2023. Controls on sediment storage in wide mountain valleys — a case study from Srinagar (Garhwal) valley, NW Himalaya. Geosciences Journal 27, 23-43, http://doi.org/10.1007/s12303-022-0023-0

Elznicová, J., Kiss, T., von Suchodoletz, H., Bartyik, T., Sipos, G., Lenďáková, Z., Fačevicová, K., Pavlů, I., Kovárník, J., Matys Grygar, T., 2023. Was the termination of the Jizera River meandering during the Late Holocene caused by anthropogenic or climatic forcing? Earth Surface Processes and Landforms 48, 669-686, http://doi.org/10.1002/esp.5509

Feng, Z., Peng, T., Ma, Z., Han, B., Wang, H., Guo, B., Zhao, Z., Zhang, J., Song, C., Hu, Z., 2022. Contrasting responses of rivers with different sizes to extrinsic changes in the northeastern Tibetan Plateau. Journal of Asian Earth Sciences 233, 105269, http://doi.org/10.1016/j.jseaes.2022.105269

Forman, S.L., Wu, Z., Wiest, L., Marin, L., Mayhack, C., 2023. Late Quaternary fluvial and aeolian depositional environments for the western Red River, Southern Great Plains, USA. Quaternary Research 115, 3-24, http://doi.org/10.1017/qua.2023.15

Ghilardi, M., Kinnaird, T., Kouli, K., Bicket, A., Crest, Y., Demory, F., Delanghe, D., Fachard, S., Sanderson, D., 2022. Reconstructing the Fluvial History of the Lilas River (Euboea Island, Central West Aegean Sea) from the Mycenaean Times to the Ottoman Period. Geosciences 12, http://doi.org/10.3390/geosciences12050204

Guyez, A., Bonnet, S., Reimann, T., Carretier, S., Wallinga, J., 2023. A novel approach to quantify sediment transfer and storage in rivers—testing feldspar single-grain pirir analysis and numerical simulations. Journal of Geophysical Research: Earth Surface 128, e2022JF006727, http://doi.org/10.1029/2022JF006727

Ishii, Y., 2024. IRSL and post-IR IRSL dating of multi-grains, single grains, and cobble surfaces to constrain fluvial responses to climate changes during the last glacial period in the Tokachi Plain, northern Japan. Quaternary Geochronology 79, 101486, http://doi.org/10.1016/j.quageo.2023.101486

Jakhmola, R.P., Dash, C., Singh, S., Patel, N.K., Verma, A.K., Pati, P., Awasthi, A.K., Sarma, J.N., 2023. Holocene landscape evolution of the Brahmaputra River valley in the upper Assam Basin (India): Deduced from the soil-geomorphic studies. Quaternary Science Reviews 316, 108243, http://doi.org/10.1016/j.quascirev.2023.108243

Kaushik, S., Sundriyal, Y., Chauhan, N., Rana, N., Sharma, S., 2023. Reconstructing the pattern of late Quaternary climate through sediment-landform assemblages in the Dhauli Ganga valley (upper Ganga catchment), India. Geomorphology 432, 108708, http://doi.org/10.1016/j.geomorph.2023.108708

Liang, H., Zhang, K., Li, Z., Fu, J., Yu, Z., Xiong, J., Li, X., Ma, Z., Huang, P., Li, Z., Zhang, Y., Hui, G., Tian, Q., Wang, W., Zheng, W., Zhang, P., 2023. How headward erosion breaches upstream paleolakes: Insights from dated longitudinal fluvial terrace correlations within the Sanmen Gorge, Yellow River. GSA Bulletin 135, 1602-1617, http://doi.org/10.1130/B36537.1

Liu, S.-H., Lüthgens, C., Hardt, J., Hebenstreit, R., Böse, M., Frechen, M., 2023. Late Quaternary formation of the Miaoli Tableland in northwest Taiwan, an interplay of tectonic uplift and fluvial processes dated by OSL. Quaternary Research 112, 128-149, http://doi.org/10.1017/qua.2022.52

Lüthgens, C., Luciani, M., Prochazka, S., Firla, G., Hoelzmann, P., Abualhassan, A.M., 2023. Watering the desert: Oasis hydroarchaeology, geochronology and functionality in Northern Arabia. The Holocene 33, 562-580, http://doi.org/10.1177/09596836231157292

Mahadev, Jaiswal, M.K., Shivsager, V., Singh, S., K, A., Singh, A.K., 2022. Late quaternary evolution of lower Kaveri and adjoining river basins in Tamil Nadu, Southern India: A combined approach using remote sensing and optical dating of fluvial records. Environmental Challenges 9, 100595, http://doi.org/10.1016/j.envc.2022.100595

Mao, P., Guo, Y., Liu, T., 2023. Holocene extreme palaeofloods recorded by slackwater deposits along the Jiacha Gorge of the Yarlung Tsangpo River valley, southern Tibetan Plateau. CATENA 231, 107360, http://doi.org/10.1016/j.catena.2023.107360

Mueller, D., Raith, K., Bretzke, K., Fülling, A., Parker, A.G., Parton, A., Preston, G.W., Jasim, S., Yousif, E., Preusser, F., 2023. Luminescence chronology of fluvial and aeolian deposits from the Emirate of Sharjah, UAE. Quaternary Research 112, 111-127, http://doi.org/10.1017/qua.2022.51

Ott, R.F., Scherler, D., Wegmann, K.W., D'Arcy, M.K., Pope, R.J., Ivy-Ochs, S., Christl, M., Vockenhuber, C., Rittenour, T.M., 2023. Paleo-denudation rates suggest variations in runoff drove aggradation during last

glacial cycle, Crete, Greece. Earth Surface Processes and Landforms 48, 386-405, http://doi.org/10.1002/esp.5492

Pears, B., Brown, A.G., Toms, P.S., Wood, J., Pennington, B.T., Jones, R., 2023. Rapid laminated clastic alluviation associated with increased Little Ice Age flooding co-driven by climate variability and historic land-use in the middle Severn catchment, UK. The Holocene 33, 1474-1488, http://doi.org/10.1177/09596836231197740

Rodrigues, K., Keen-Zebert, A., Shepherd, S., Hudson, M.R., Bitting, C.J., Johnson, B.G., Langston, A., 2023. The role of lithology and climate on bedrock river incision and terrace development along the Buffalo National River, Arkansas. Quaternary Research 115, 179-193, http://doi.org/10.1017/qua.2023.16

Saha, U.D., Bhattacharya, S., Bhattacharya, H.N., Islam, A., Jaiswal, M., Narzary, B., Dutt, S., 2023. Development of a hyper-avulsive river course during the Holocene on the Himalayan frontal plains. CATENA 231, 107279, http://doi.org/10.1016/j.catena.2023.107279

Shen, Q., Zhou, Y., Xu, Y., Lai, Y., Yan, X., Huang, X., Liu, X., Zhong, J., Zhu, S., Li, Z., Lai, Z., 2023. Late Quaternary river evolution and its response to climate changes in the upper Mekong River of the Qinghai–Tibetan Plateau. Geomorphology 442, 108920, http://doi.org/10.1016/j.geomorph.2023.108920

Sridhar, A., Bhattacharya, F., Vanik, N., Maurya, D.M., Chamyal, L.S., 2022. Late Pleistocene history of aggradation and incision within a bedrock gorge, Narmada River, central India: implications for resurgent tectonic activity and changing climate. Journal of Quaternary Science 37, 1371-1387, http://doi.org/10.1002/jqs.3453

Sun, A., Li, H., Zhang, S., Cao, H., Qiu, M., Wang, Y., Liu, B., Zhao, H., Dong, G., 2023. Impact of climate-driven oasis evolution on human settlement in the Baiyang River Basin, northwest China, Hami, during the middle to late Holocene. Palaeogeography, Palaeoclimatology, Palaeoecology 622, 111602, http://doi.org/10.1016/j.palaeo.2023.111602

Sweeney, M.R., McDonald, E.V., Chabela, L.P., Hanson, P.R., 2020. The role of eolian-fluvial interactions and dune dams in landscape change, late Pleistocene–Holocene, Mojave Desert, USA. GSA Bulletin 132, 2318-2332, http://doi.org/10.1130/B35434.1

Tuzlak, D., Pederson, J., Bufe, A., Rittenour, T., 2021. Patterns of incision and deformation on the southern flank of the Yellowstone hotspot from terraces and topography. GSA Bulletin 134, 1319-1333, http://doi.org/10.1130/B35923.1

Viveen, W., Sanjurjo-Sanchez, J., Baby, P., del Rosario González-Moradas, M., 2021. An assessment of competing factors for fluvial incision: An example of the late Quaternary exorheic Moyobamba basin, Peruvian Subandes. Global and Planetary Change 200, 103476, http://doi.org/10.1016/j.gloplacha.2021.103476

Viveen, W., Sanjurjo-Sanchez, J., Rosas, M.A., Vanacker, V., Villegas-Lanza, J.C., 2022. Heinrich events and tectonic uplift as possible drivers for late Quaternary fluvial dynamics in the western Peruvian Andes. Global and Planetary Change 218, 103972, http://doi.org/10.1016/j.gloplacha.2022.103972

Wang, P., Wang, H., Liu, T., Hu, G., Qin, J., Yuan, R., 2024. Sedimentary records of megafloods in the Yarlung Tsangpo Gorge in the eastern Himalaya since the Last Glacial Period. Quaternary Science Reviews 324, 108436, http://doi.org/10.1016/j.quascirev.2023.108436

Wang, Z., Yin, J.-J., Hao, X., Yang, H., Wu, X., Lan, G., Tang, W., 2023. Enhanced debris flow activities in the subtropical mountainous catchment of South China during early Marine Isotope Stage 3. CATENA 231, 107331, http://doi.org/10.1016/j.catena.2023.107331

Woor, S., Thomas, D.S.G., Durcan, J.A., Burrough, S.L., Parton, A., 2023. The aggradation of alluvial fans in response to monsoon variability over the last 400 ka in the Hajar Mountains, south-east Arabia. Quaternary Science Reviews 322, 108384, http://doi.org/10.1016/j.quascirev.2023.108384

Xiao, Q., Zhang, Y., Wang, N., Huang, C.C., Qiu, H., Zhu, Y., Wang, H., Jia, Y.-n., Chen, D., Wang, C., Wang, S., Storozum, M., 2022. Paleochannel of the Yellow River within the Zoige Basin and its environmental significance on the NE Tibetan Plateau. Science of The Total Environment 853, 158242, http://doi.org/10.1016/j.scitotenv.2022.158242

Yorke, L., Chiverrell, R.C., Schwenninger, J.L., 2024. Lateglacial and early Holocene evolution of the Tyne Valley in response to climatic shifts and possible paraglacial landscape legacies. Geomorphology 446, 109007, http://doi.org/10.1016/j.geomorph.2023.109007

Zhang, A., Gao, Q., Mostafizur Rahman, S., Mahbubul Alam, M., Guo, Y., Chen, Y., Chen, J., Wang, H., Wang, P., Zhang, J., Yi, C., Hu, G., 2023. Luminescence fingerprints fluvial sediment transport from the Tibetan Plateau to the Bangladesh Delta. Earth and Planetary Science Letters 622, 118387, http://doi.org/10.1016/j.epsl.2023.118387

- glacial and periglacial

Alexanderson, H., Hättestrand, M., Lindqvist, M.A., Sigfúsdóttir, T., 2022. MIS 3 age of the Veiki moraine in N Sweden – Dating the landform record of an intermediate-sized ice sheet in Scandinavia. Arctic, Antarctic, and Alpine Research 54, 239-261, http://doi.org/10.1080/15230430.2022.2091308

Balco, G., Brown, N., Nichols, K., Venturelli, R.A., Adams, J., Braddock, S., Campbell, S., Goehring, B., Johnson, J.S., Rood, D.H., Wilcken, K., Hall, B., Woodward, J., 2023. Reversible ice sheet thinning in the Amundsen Sea Embayment during the Late Holocene. The Cryosphere 17, 1787-1801, http://doi.org/10.5194/tc-17-1787-2023

Borisova, O., Konstantinov, E., Utkina, A., Baranov, D., Panin, A., 2022. On the existence of a large proglacial lake in the Rostov-Kostroma lowland, north-central European Russia. Journal of Quaternary Science 37, 1442-1459, http://doi.org/10.1002/jqs.3454

Borodin, A.V., Markova, E.A., Korkin, S.E., Trofimova, S.S., Zinovyev, E.V., Isypov, V.A., Yalkovskaya, L.E., Kurbanov, R.N., 2023. Late Middle Pleistocene sequences in the lower Ob' and Irtysh (West Siberia) and new multi-proxy records of terrestrial environmental change. Quaternary International 671, 15-32, http://doi.org/10.1016/j.quaint.2023.07.009

Das, S., Murari, M.K., Sharma, M.C., Saini, R., Jaiswal, M.K., Kumar, P.V., Kumar, P., 2023. Reconstraining the Quaternary glacial history of Lahaul Himalaya, northern India. Quaternary Science Reviews 316, 108258, http://doi.org/10.1016/j.quascirev.2023.108258

Dey, S., Chauhan, N., Mahala, M.K., Chakravarti, P., Vashistha, A., Jain, V., Ray, J.S., 2022. Dominant role of deglaciation in Late Pleistocene–Early Holocene sediment aggradation in the Upper Chenab valley, NW Himalaya. Quaternary Research 113, 122-133, http://doi.org/10.1017/qua.2022.57

Erber, N.R., Kehew, A.E., Schaetzl, R.J., Gillespie, R., Sultan, M.E., Esch, J., Yellich, J., Brandon Curry, B., Huot, S., Abotalib, A.Z., 2023. Revisiting the timing of Saginaw lobe ice retreat and implications for drainage adjustments across southern Michigan, USA. CATENA 233, 107510, http://doi.org/10.1016/j.catena.2023.107510

Gibbard, P.L., Bateman, M.D., Leathard, J., West, R.G., 2021. Luminescence dating of a late Middle Pleistocene glacial advance in eastern England. Netherlands Journal of Geosciences 100, e18, http://doi.org/10.1017/njg.2021.13

Hodder, T.J., Gauthier, M.S., Ross, M., Lian, O.B., 2023. Was there a nonglacial episode in the western Hudson Bay Lowland during Marine Isotope Stage 3? Quaternary Research 116, 148-161, http://doi.org/10.1017/qua.2023.35

Karpukhina, N.V., Karevskaya, I.A., Borisova, O.K., Konstantinov, E.A., Kurbanov, R.N., Zakharov, A.L., Filippova, K.G., Zazovskaya, E.P., 2022. Evolution of a proglacial lake in the Izborsko-Malskaya Valley, Russia, in the Late Glacial. Journal of Quaternary Science 37, 1460-1479, http://doi.org/10.1002/jqs.3455

Mangerud, J., Alexanderson, H., Birks, H.H., Paus, A., Perić, Z.M., Svendsen, J.I., 2023. Did the Eurasian ice sheets melt completely in early Marine Isotope Stage 3? New evidence from Norway and a synthesis for Eurasia. Quaternary Science Reviews 311, 108136, http://doi.org/10.1016/j.quascirev.2023.108136

Moska, P., Sokołowski, R.J., Zieliński, P., Jary, Z., Raczyk, J., Mroczek, P., Szymak, A., Krawczyk, M., Skurzyński, J., Poręba, G., Łopuch, M., Tudyka, K., 2023. An impact of short-term climate oscillations in the Late Pleniglacial and Lateglacial interstadial on sedimentary processes and the pedogenic record in central Poland. Annals of the American Association of Geographers 113, 46-70, http://doi.org/10.1080/24694452.2022.2094325

Pfander, J., Schlunegger, F., Serra, E., Gribenski, N., Garefalakis, P., Akçar, N., 2022. Glaciofluvial sequences recording the Birrfeld Glaciation (MIS 5d–2) in the Bern area, Swiss Plateau. Swiss Journal of Geosciences 115, 12, http://doi.org/10.1186/s00015-022-00414-z

Rasmussen, C.F., Christiansen, H.H., Buylaert, J.-P., Cunningham, A., Schneider, R., Knudsen, M.F., Stevens, T., 2023. High-resolution OSL dating of loess in Adventdalen, Svalbard: Late Holocene dust activity and permafrost development. Quaternary Science Reviews 310, 108137, http://doi.org/10.1016/j.quascirev.2023.108137

Sharma, S., Shukla, A.D., 2024. Mid-Holocene climate-glacier relationship inferred from landforms and relict lake sequence, Southern Zanskar ranges, NW Himalaya. Geomorphology 444, 108953, http://doi.org/10.1016/j.geomorph.2023.108953

Šujan, M., Rybár, S., Thamó-Bozsó, E., Klučiar, T., Tibenský, M., Sebe, K., 2022. Collapse wedges in periglacial eolian sands evidence Late Pleistocene paleoseismic activity of the Vienna Basin Transfer Fault (western Slovakia). Sedimentary Geology 431, 106103, http://doi.org/10.1016/j.sedgeo.2022.106103

Turu, V., Peña-Monné, J.L., Cunha, P.P., Jalut, G., Buylaert, J.-P., Murray, A.S., Bridgland, D., Faurschou-Knudsen, M., Oliva, M., Carrasco, R.M., Ros, X., Turu-Font, L., Ventura Roca, J., 2023. Glacial–

interglacial cycles in the south-central and southeastern Pyrenees since ~180 ka (NE Spain–Andorra–S France). Quaternary Research 113, 1-28, http://doi.org/10.1017/qua.2022.68

Xie, J., Yang, T., Zhou, S., Xu, L., Ou, X., Hu, G., 2023. Glacial fluctuations during the Last Glacial Maximum and Lateglacial in the Zhuxi and Songlong valleys, eastern Nyainqêntanglha Range, southeastern Tibet. Journal of Quaternary Science 38, 580-596, http://doi.org/10.1002/jqs.3484

- lacustrine

Gong, Z., Li, Q., Luo, M., Dai, C., Peng, H., 2023. Sedimentary facies and chronological study for a Late Pleistocene sand layer with swash cross bedding within a sand hill at north of Poyang Lake, as inferred from sedimentary structure and optical dating of K-feldspar and quartz grains. Quaternary International 673, 29-39, http://doi.org/10.1016/j.quaint.2023.10.001

Hudson, A.M., Quade, J., Holliday, V.T., Fenerty, B., Bright, J.E., Gray, H.J., Mahan, S.A., 2023. Paleohydrologic history of pluvial lake San Agustin, New Mexico: Tracking changing effective moisture in southwest North America through the last glacial transition. Quaternary Science Reviews 310, 108110, http://doi.org/10.1016/j.quascirev.2023.108110

Sagwal, S., Kumar, A., Sharma, C.P., Srivastava, P., Agarwal, S., Bhushan, R., 2023. Late-Holocene hydrological variability from the NW Himalaya and southwestern Tibetan Plateau: Paleo-salinity records from Pangong Tso. The Holocene 33, 842-859, http://doi.org/10.1177/09596836231163486

Wang, P., Wang, H., Hu, G., Ge, Y., Liu, T., Xu, B., 2023. Reconstructing post-mid Pleistocene glacial-dammed paleolakes in the Tsangpo Gorge, southeastern Tibetan Plateau. Quaternary Science Reviews 314, 108228, http://doi.org/10.1016/j.quascirev.2023.108228

Yi, S., Wang, X., Xu, Z., Wu, J., Lu, H., 2023. Late Quaternary hydroclimatic variations in the hyper-arid Dunhuang Basin, northwestern China. Palaeogeography, Palaeoclimatology, Palaeoecology 626, 111693, http://doi.org/10.1016/j.palaeo.2023.111693

Zhang, Z., Shen, Z., Zhang, S., Chen, J., Chen, S., Li, D., Zhang, S., Liu, X., Wu, D., Sheng, Y., Tang, Q., Chen, F., Liu, J., 2022. Lake level evidence for a mid-Holocene East Asian summer monsoon maximum and the impact of an abrupt late-Holocene drought event on prehistoric cultures in north-central China. The Holocene 33, 382-399, http://doi.org/10.1177/09596836221145362

Zheng, J., Zhang, J., Zhang, B., Wang, Y., Gu, D., Feng, L., Wang, H., 2023. Quaternary evolution of the Dunhuang paleolake and its controlling factors in the northeastern Tibetan Plateau. Geomorphology 438, 108814, http://doi.org/10.1016/j.geomorph.2023.108814

- loess

Bosq, M., Kreutzer, S., Bertran, P., Lanos, P., Dufresne, P., Schmidt, C., 2023. Last Glacial loess in Europe: luminescence database and chronology of deposition. Earth System Science Data 15, 4689-4711, http://doi.org/10.5194/essd-15-4689-2023

Constantin, D., Mason, J.A., Veres, D., Hambach, U., Panaiotu, C., Zeeden, C., Zhou, L., Marković, S.B., Gerasimenko, N., Avram, A., Tecsa, V., Groza-Sacaciu, S.M., del Valle Villalonga, L., Begy, R., Timar-Gabor, A., 2021. OSL-dating of the Pleistocene-Holocene climatic transition in loess from China, Europe and North America, and evidence for accretionary pedogenesis. Earth-Science Reviews 221, 103769, http://doi.org/10.1016/j.earscirev.2021.103769

Dave, A.K., Lisá, L., Scardia, G., Nigmatova, S., Fitzsimmons, K.E., 2023. The patchwork loess of Central Asia: Implications for interpreting aeolian dynamics and past climate circulation in piedmont regions. Journal of Quaternary Science 38, 526-543, http://doi.org/10.1002/jqs.3493

Li, G., Wang, Y., Yan, Z., Qin, C., Ding, W., Yang, H., Wang, X., Zhang, X., 2023. High-resolution luminescence chronology of loess-paleosols reveals East Asian summer monsoon and winter monsoon variation in Hexi Corridor during the past 25 kyr. Palaeogeography, Palaeoclimatology, Palaeoecology 627, 111743, http://doi.org/10.1016/j.palaeo.2023.111743

Li, Q., Li, P., Liu, X., Chen, Z., Liu, L., Liu, W., Luo, Y., Zhou, J., Wen, C., Yang, S., 2023. Aeolian process and climatic changes in loess records from the eastern Tibetan Plateau: Implications for paleoenvironmental dynamics since MIS 3. CATENA 231, 107361, http://doi.org/10.1016/j.catena.2023.107361

Li, Y., Zhang, R., Long, H., Cheng, P., Kemp, D.B., Zhang, Z., Huang, C., Hou, M., Li, Y., Jia, S., Wang, Z., Tan, L., 2023. Climate changes in the Hexi Corridor, western China over the past 13.3 ka. Palaeogeography, Palaeoclimatology, Palaeoecology 622, 111605, http://doi.org/10.1016/j.palaeo.2023.111605

Schmidt, A.H., Collins, B.D., Keen-Zebert, A., d'Alpoim Guedes, J., Hein, A., Womack, A., McGuire, C., Feathers, J., Persico, L., Fiallo, D., Tang, Y., Simonson, B., 2023. Implications of the loess record for Holocene climate and human settlement in Heye Catchment, Jiuzhaigou, eastern Tibetan Plateau, Sichuan, China. Quaternary Research 112, 36-50, http://doi.org/10.1017/qua.2022.44

Schulze, T., Schwahn, L., Fülling, A., Zeeden, C., Preusser, F., Sprafke, T., 2022. Investigating the loess–palaeosol sequence of Bahlingen-Schönenberg (Kaiserstuhl), southwestern Germany, using a multi-methodological approach. E&G Quaternary Science Journal 71, 145-162, http://doi.org/10.5194/egqsj-71-145-2022

Schwahn, L., Schulze, T., Fülling, A., Zeeden, C., Preusser, F., Sprafke, T., 2023. Multi-method study of the Middle Pleistocene loess–palaeosol sequence of Köndringen, SW Germany. E&G Quaternary Science Journal 72, 1-21, http://doi.org/10.5194/egqsj-72-1-2023

Shah, R.A., Achyuthan, H., Lone, A.M., Jaiswal, M.K., Paul, D., 2021. Constraining the timing and deposition pattern of loess-palaeosol sequences in Kashmir Valley, Western Himalaya: Implications to paleoenvironment studies. Aeolian Research 49, 100660, http://doi.org/10.1016/j.aeolia.2020.100660

Zhang, J., Li, S.-H., Sun, J., Lü, T., Zhou, X., Hao, Q., 2023. Quartz luminescence sensitivity variation in the Chinese loess deposits: the potential role of wildfires. Journal of Quaternary Science 38, 49-60, http://doi.org/10.1002/jqs.3462

Zhang, J., Tsukamoto, S., Long, H., 2023. Testing the potential of pulsed post-IR IRSL dating on Chinese loess deposits. Quaternary Geochronology 78, 101469, http://doi.org/10.1016/j.quageo.2023.101469

Zhang, S., Yang, S., Jiang, W., Huang, X., Wang, Y., Sun, M., Guo, L., Yang, X., Ding, Z., 2023. BrGDGTs-based temperature and hydrological reconstruction from loess-paleosol deposits in the Eastern European Plain since 200 ka. Quaternary Science Reviews 316, 108275, http://doi.org/10.1016/j.quascirev.2023.108275

Zhang, Z., Zheng, Z., Meng, X., Lai, Z., Hou, Y., Ji, J., 2023. Gradually increasing precipitation since 20 ka as evidenced by loess dolomite abundance in the Ili Basin, Central Asia. CATENA 232, 107420, http://doi.org/10.1016/j.catena.2023.107420

- marine

Gao, L., Li, J., Hu, B., Yi, L., Tamura, T., Long, H., 2022. Luminescence dating of a sedimentary sequence in the eastern North Yellow Sea. Marine and Petroleum Geology 138, 105543, http://doi.org/10.1016/j.marpetgeo.2022.105543

- soil

Puyrigaud, J., Bertran, P., Lebrun, B., Lahaye, C., Guerin, G., Limondin-Lozouet, N., 2023. Last Interglacial–Glacial sequence of palaeosols and calcareous slope deposits at Verteuil (Charente, southwest France). Journal of Quaternary Science 38, 1321-1336, http://doi.org/10.1002/jqs.3538

- surface exposure dating

Ageby, L., Brill, D., Angelucci, D.E., Brückner, H., Klasen, N., 2023. Investigating optical dating of carbonate-rich cobbles from a river terrace: A pilot study from the Mula Valley, Spain. Radiation Measurements 166, 106962, http://doi.org/10.1016/j.radmeas.2023.106962

al Khasawneh, S., Murray, A., Gebel, H.G.K., 2024. Direct dating of a major rockfall at the Ba'ja Neolithic site (Jordan) using rock surface luminescence. Quaternary Geochronology 79, 101475, http://doi.org/10.1016/j.quageo.2023.101475

Andričević, P., Sellwood, E.L., Freiesleben, T., Hidy, A.J., Kook, M., Eppes, M.C., Jain, M., 2023. Dating fractures using luminescence. Earth and Planetary Science Letters 624, 118461, http://doi.org/10.1016/j.epsl.2023.118461

Balco, G., Brown, N., Nichols, K., Venturelli, R.A., Adams, J., Braddock, S., Campbell, S., Goehring, B., Johnson, J.S., Rood, D.H., Wilcken, K., Hall, B., Woodward, J., 2023. Reversible ice sheet thinning in the Amundsen Sea Embayment during the Late Holocene. The Cryosphere 17, 1787-1801, http://doi.org/10.5194/tc-17-1787-2023

Bench, T., Sanderson, D., Feathers, J., Warfield, E., 2023. Investigating the use of two-dimensional OSL laser scanning instruments and energy-dispersive x-ray spectroscopy for OSL exposure dating. Radiation Measurements 167, 106999, http://doi.org/10.1016/j.radmeas.2023.106999

Freiesleben, T.H., Thomsen, K.J., Sellwood, E., Liu, J., Murray, A.S., 2023. Testing new kinetic models and calibration methods for Rock Surface Luminescence Exposure dating using controlled experiments. Radiation Measurements 169, 107033, http://doi.org/10.1016/j.radmeas.2023.107033

Ishii, Y., 2024. IRSL and post-IR IRSL dating of multi-grains, single grains, and cobble surfaces to constrain fluvial responses to climate changes during the last glacial period in the Tokachi Plain, northern Japan. Quaternary Geochronology 79, 101486, http://doi.org/10.1016/j.quageo.2023.101486

Liu, Q., Chen, J., Qin, J., Di, N., Luo, M., Yang, H., Liu, J., 2023. Zeroing of IRSL signals in cobbles surfaces from a modern river floodplain in the Manas river, Tian Shan. Quaternary International 672, 52-62, http://doi.org/10.1016/j.quaint.2023.09.001

Luo, M., Chen, J., Owen, L.A., Qin, J., Yin, J., Yang, H., Liu, J., Gong, Z., Luo, J., 2022. A novel approach for reconstructing slip histories for bedrock fault scarps using rock surface luminescence dating. Geophysical Research Letters 49, e2022GL099526, http://doi.org/10.1029/2022GL099526

Moayed, N.K., Sohbati, R., Murray, A.S., Rades, E.F., Fattahi, M., Ruiz López, J.F., 2023. Rock surface luminescence dating of prehistoric rock art from central Iberia. Archaeometry 65, 319-334, http://doi.org/10.1111/arcm.12826

Polymeris, G.S., Liritzis, I., Iliopoulos, I., Xanthopoulou, V., Bednarik, R.G., Kumar, G., Vafiadou, A., 2023. Constraining the minimum age of Daraki-Chattan rock art in India by OSL dating and petrographic analyses. Quaternary Geochronology 78, 101472, http://doi.org/10.1016/j.quageo.2023.101472

Sohbati, R., Hippe, K., 2023. OSL-14C-10Be: A novel composite geochronometer for simultaneous quantification of timing and magnitude of change in bedrock outcrop erosion rate. Earth Surface Processes and Landforms 48, 322-331, http://doi.org/10.1002/esp.5487

- tephra (and volcanic related)

Anil, D., Devi, M., Blinkhorn, J., Smith, V., Sanghode, S., Mahesh, V., Khan, Z., Ajithprasad, P., Chauhan, N., 2023. Youngest Toba Tuff deposits in the Gundlakamma River basin, Andhra Pradesh, India and their role in evaluating Late Pleistocene behavioral change in South Asia. Quaternary Research 115, 134-145, http://doi.org/10.1017/qua.2023.13

Archaeology applications

al Khasawneh, S., Murray, A., Gebel, H.G.K., 2024. Direct dating of a major rockfall at the Ba'ja Neolithic site (Jordan) using rock surface luminescence. Quaternary Geochronology 79, 101475, http://doi.org/10.1016/j.quageo.2023.101475

al Khasawneh, S., Schmidt, K., Murray, A., Thompson, W., 2023. Luminescence dating of anthropogenic deposits from Tall Zarʿa in the Jordan Valley. Archaeometry 65, 972-986, http://doi.org/10.1111/arcm.12871

Archer, W., Presnyakova, D., Aldeias, V., Colarossi, D., Hutten, L., Lauer, T., Porraz, G., Rossouw, L., Shaw, M., 2023. Late Acheulean occupations at Montagu Cave and the pattern of Middle Pleistocene behavioral change in Western Cape, southern Africa. Journal of Human Evolution 184, 103435, http://doi.org/10.1016/j.jhevol.2023.103435

Barham, L., Duller, G.A.T., Candy, I., Scott, C., Cartwright, C.R., Peterson, J.R., Kabukcu, C., Chapot, M.S., Melia, F., Rots, V., George, N., Taipale, N., Gethin, P., Nkombwe, P., 2023. Evidence for the earliest structural use of wood at least 476,000 years ago. Nature, http://doi.org/10.1038/s41586-023-06557-9

Cheliz, P.M., Giannini, P.C.F., Moreno de Sousa, J.C., Ladeira, F.S.B., Rodrigues, J.A., Mingatos, G.S., Pupim, F.N., Mineli, T.D., Galhardo, D., Rodrigues, R.A., 2023. Early anthropic occupation and geomorphological changes in South America: human–environment interactions and OSL data from the Rincão I site, southeastern Brazil. Journal of Quaternary Science 38, 685-701, http://doi.org/10.1002/jqs.3505

Demeter, F., Zanolli, C., Westaway, K.E., Joannes-Boyau, R., Duringer, P., Morley, M.W., Welker, F., Rüther, P.L., Skinner, M.M., McColl, H., Gaunitz, C., Vinner, L., Dunn, T.E., Olsen, J.V., Sikora, M., Ponche, J.-L., Suzzoni, E., Frangeul, S., Boesch, Q., Antoine, P.-O., Pan, L., Xing, S., Zhao, J.-X., Bailey, R.M., Boualaphane, S., Sichanthongtip, P., Sihanam, D., Patole-Edoumba, E., Aubaile, F., Crozier, F., Bourgon, N., Zachwieja, A., Luangkhoth, T., Souksavatdy, V., Sayavongkhamdy, T., Cappellini, E., Bacon, A.-M., Hublin, J.-J., Willerslev, E., Shackelford, L., 2022. A Middle Pleistocene Denisovan molar from the Annamite Chain of northern Laos. Nature Communications 13, 2557, http://doi.org/10.1038/s41467-022-29923-z

Demuro, M., Arnold, L.J., González-Urquijo, J., Lazuen, T., Frochoso, M., 2023. Chronological constraint of Neanderthal cultural and environmental changes in southwestern Europe: MIS 5–MIS 3 dating of the Axlor site (Biscay, Spain). Journal of Quaternary Science 38, 891-920, http://doi.org/10.1002/jqs.3527

Duval, M., Sahnouni, M., Parés, J.M., Zhao, J.-x., Grün, R., Abdessadok, S., Pérez-González, A., Derradji, A., Harichane, Z., Mazouni, N., Boulaghraief, K., Cheheb, R.C., van der Made, J., 2023. On the age of Ain Hanech Oldowan locality (Algeria): First numerical dating results. Journal of Human Evolution 180, 103371, http://doi.org/10.1016/j.jhevol.2023.103371

Eixea, A., Bel, M.Á., Carrión Marco, Y., Ferrer-García, C., Guillem, P.M., Martínez-Alfaro, Á., Martínez-Varea, C.M., Moya, R., Rodrigues, A.L., Dias, M.I., Russo, D., Sanchis, A., 2023. A multi-proxy study from new excavations in the Middle Palaeolithic site of Cova del Puntal del Gat (Benirredrà, València, Spain). Comptes Rendus Palevol 10, http://doi.org/10.5852/cr-palevol2023v22a10

Esiana, B.O.I., Oram, R.D., 2023. Soil and spatial analyses in the assessment of the focal point of the extinct medieval royal burgh of Roxburgh. Journal of Archaeological Science: Reports 50, 104104, http://doi.org/10.1016/j.jasrep.2023.104104

Feathers, J., 2023. The contributions of luminescence dating of sediments to understanding the first settlement of the Americas. PaleoAmerica 9, 81-114, http://doi.org/10.1080/20555563.2023.2234740

Fernández, A.F., Carvalho, P.C., Cristóvão, J., Sanjurjo-Sánchez, J., Dias, P., 2019. Dating the early Christian baptisteries from Idanha-a-Velha—the Suebi-Visigothic Egitania: stratigraphy, radiocarbon and OSL. Archaeological and Anthropological Sciences 11, 5691-5704, http://doi.org/10.1007/s12520-019-00901-9

Fourcade, T., Sánchez Goñi, M.F., Lahaye, C., Rossignol, L., Philippe, A., 2022. Environmental changes in SW France during the Middle to Upper Paleolithic transition from the pollen analysis of an eastern North Atlantic deep-sea core. Quaternary Research 110, 147-164, http://doi.org/10.1017/qua.2022.21

Freidline, S.E., Westaway, K.E., Joannes-Boyau, R., Duringer, P., Ponche, J.-L., Morley, M.W., Hernandez, V.C., McAllister-Hayward, M.S., McColl, H., Zanolli, C., Gunz, P., Bergmann, I., Sichanthongtip, P., Sihanam, D., Boualaphane, S., Luangkhoth, T., Souksavatdy, V., Dosseto, A., Boesch, Q., Patole-Edoumba, E., Aubaile, F., Crozier, F., Suzzoni, E., Frangeul, S., Bourgon, N., Zachwieja, A., Dunn, T.E., Bacon, A.-M., Hublin, J.-J., Shackelford, L., Demeter, F., 2023. Early presence of Homo sapiens in Southeast Asia by 86–68 kyr at Tam Pà Ling, Northern Laos. Nature Communications 14, 3193, http://doi.org/10.1038/s41467-023-38715-y

Fusco, D.A., Arnold, L.J., Gully, G.A., Levchenko, V.A., Jacobsen, G.E., Prideaux, G.J., 2023. Revisiting the late Quaternary fossiliferous infills of Cathedral Cave, Wellington Caves (central eastern New South Wales, Australia). Journal of Quaternary Science 38, 505-525, http://doi.org/10.1002/jqs.3497

Groucutt, H.S., White, T.S., Scerri, E.M.L., Andrieux, E., Clark-Wilson, R., Breeze, P.S., Armitage, S.J., Stewart, M., Drake, N., Louys, J., Price, G.J., Duval, M., Parton, A., Candy, I., Carleton, W.C., Shipton, C., Jennings, R.P., Zahir, M., Blinkhorn, J., Blockley, S., Al-Omari, A., Alsharekh, A.M., Petraglia, M.D., 2021. Multiple hominin dispersals into Southwest Asia over the past 400,000 years. Nature 597, 376-380, http://doi.org/10.1038/s41586-021-03863-y

Grün, R., Pike, A., McDermott, F., Eggins, S., Mortimer, G., Aubert, M., Kinsley, L., Joannes-Boyau, R., Rumsey, M., Denys, C., Brink, J., Clark, T., Stringer, C., 2020. Dating the skull from Broken Hill, Zambia, and its position in human evolution. Nature 580, 372-375, http://doi.org/10.1038/s41586-020-2165-4

Grün, R., Stringer, C., 2023. Direct dating of human fossils and the ever-changing story of human evolution. Quaternary Science Reviews 322, 108379, http://doi.org/10.1016/j.quascirev.2023.108379

Guibert, P., Guérin, G., Javel, J.-B., Urbanová, P., 2020. Modeling light exposure of quartz grains during mortar making: Consequences for optically stimulated luminescence dating. Radiocarbon 62, 693-711, http://doi.org/10.1017/RDC.2020.34

Han, F., Bahain, J.-J., Shao, Q., Sun, X., Voinchet, P., Xiao, P., Huang, M., Li, M., Yin, G., 2022. The Chronology of Early Human Settlement in Three Gorges Region, China—Contribution of Coupled Electron Spin Resonance and Uranium-Series Dating Method. Frontiers in Earth Science 10, http://doi.org/10.3389/feart.2022.939766

Hervé, G., Guibert, P., Meunier, H., Monteil, M., Dufresne, P., Lanos, P., Oberlin, C., Ben Aissa, G., 2023. Chronology of the Late Roman Antiquity walls of Le Mans (France) by OSL, archaeomagnetism and radiocarbon. Journal of Archaeological Science: Reports 51, 104172, http://doi.org/10.1016/j.jasrep.2023.104172

Jordá Pardo, J.F., Álvarez-Alonso, D., de Andrés-Herrero, M., Ballesteros, D., Carral, P., Hevia-Carrillo, A., Sanjurjo, J., Giralt, S., Jiménez-Sánchez, M., 2023. Geomorphology, Geoarchaeology, and

Geochronology of the Upper Pleistocene Archaeological Site of El Olivo Cave (Llanera, Asturias, Northern Spain). Geosciences 13, http://doi.org/10.3390/geosciences13100301

Karimi Moayed, N., Vandenberghe, D.A.G., Verbrugge, A., Ech-Chakrouni, S., De Clercq, W., De Grave, J., 2023. Dating (early) modern hearths on a decadal to multi-annual timescale using OSL signals from heated sedimentary quartz. Journal of Archaeological Science 159, 105858, http://doi.org/10.1016/j.jas.2023.105858

Kazancı, N., Özgüneylioğlu, A., Öncel, S.M., Erturaç, M.K., Şahiner, E., 2022. Crust occurrence on a Galatian rock-cut dwelling in central Anatolia, Turkey. Geoarchaeology 37, 658-681, http://doi.org/10.1002/gea.21910

Kemp, J., Olley, J., Stout, J., Pietsch, T., Mithaka Aboriginal, C., 2022. Dating stone arrangements using optically stimulated luminescence and fallout radionuclides. Geoarchaeology 37, 439-449, http://doi.org/10.1002/gea.21902

Marquet, J.-C., Freiesleben, T.H., Thomsen, K.J., Murray, A.S., Calligaro, M., Macaire, J.-J., Robert, E., Lorblanchet, M., Aubry, T., Bayle, G., Bréhéret, J.-G., Camus, H., Chareille, P., Egels, Y., Guillaud, É., Guérin, G., Gautret, P., Liard, M., O'Farrell, M., Peyrouse, J.-B., Thamó-Bozsó, E., Verdin, P., Wojtczak, D., Oberlin, C., Jaubert, J., 2023. The earliest unambiguous Neanderthal engravings on cave walls: La Roche-Cotard, Loire Valley, France. PLOS ONE 18, e0286568, http://doi.org/10.1371/journal.pone.0286568

Martínez, G., Martínez, G.A., Owen, L.A., 2023. Human occupation, site formation, and chronostratigraphy of a mid-Holocene archaeological site at the eastern Pampa-Patagonia transition, Argentina. Quaternary Research 114, 52-68, http://doi.org/10.1017/qua.2023.8

Moayed, N.K., Sohbati, R., Murray, A.S., Rades, E.F., Fattahi, M., Ruiz López, J.F., 2023. Rock surface luminescence dating of prehistoric rock art from central Iberia. Archaeometry 65, 319-334, http://doi.org/10.1111/arcm.12826

Moayed, N.K., Vandenberghe, D., Deforce, K., Kaptijn, E., Biernacka, P., De Clercq, W., De Grave, J., 2023. OSL dating as an alternative tool for age determination of relic charcoal kilns. Archaeometry 65, 939-954, http://doi.org/10.1111/arcm.12860

Neto de Carvalho, C., Muñiz, F., Cáceres, L.M., Rodríguez-Vidal, J., Medialdea, A., Val, M.d., Cunha, P.P., García, J.M., Giles-Guzmán, F., Carrión, J.S., Belaústegui, Z., Toscano, A., Gómez, P., Galán, J.M., Belo, J., Cachão, M., Ruiz, F., Ramirez-Cruzado, S., Finlayson, G., Finlayson, S., Finlayson, C., 2023. Neanderthal footprints in the "Matalascañas trampled surface" (SW Spain): new OSL dating and Mousterian lithic industry. Quaternary Science Reviews 313, 108200, http://doi.org/10.1016/j.quascirev.2023.108200

Nightingale, S., Schilt, F., Thompson, J.C., Wright, D.K., Forman, S., Mercader, J., Moss, P., Clarke, S., Itambu, M., Gomani-Chindebvu, E., Welling, M., 2019. Late Middle Stone Age Behavior and Environments at Chaminade I (Karonga, Malawi). Journal of Paleolithic Archaeology 2, 258-297, http://doi.org/10.1007/s41982-019-00035-3

Oron, M., Roskin, J., Porat, N., Avni, Y., Aladjem, E., Yegorov, D., Vardi, J., Hovers, E., 2023. A conceptual model of multi-scale formation processes of open-air Middle Paleolithic sites in the arid Negev desert, Israel. Quaternary Research 116, 162-180, http://doi.org/10.1017/qua.2023.31

Pavlenok, K., Kot, M., Moska, P., Leloch, M., Muhtarov, G., Kogai, S., Khudjanazarov, M., Holmatov, A., Szymczak, K., 2022. New evidence for mountain Palaeolithic human occupation in the western Tian Shan piedmonts, eastern Uzbekistan. Antiquity 96, 1292-1300, http://doi.org/10.15184/aqy.2022.99

Polymeris, G.S., Liritzis, I., Iliopoulos, I., Xanthopoulou, V., Bednarik, R.G., Kumar, G., Vafiadou, A., 2023. Constraining the minimum age of Daraki-Chattan rock art in India by OSL dating and petrographic analyses. Quaternary Geochronology 78, 101472, http://doi.org/10.1016/j.quageo.2023.101472

Quinn, M., Owen, T., Flanagan, J., Westaway, K.E., 2023. An Aboriginal presence in the Sydney basin prior to the LGM; further investigations into the age and formation of the Parramatta Sand Body. Journal of Archaeological Science: Reports 51, 104195, http://doi.org/10.1016/j.jasrep.2023.104195

Ranhorn, K.L., Mavuso, S.S., Colarossi, D., Dogandžić, T., O'Brien, K., Ribordy, M., Ssebuyungo, C., Warren, S., Harris, J.W.K., Braun, D.R., Ndiema, E., 2023. By the lakeshore: Multi-scalar geoarchaeology in the Turkana Basin at GaJj17, Koobi Fora (Kenya). Quaternary Science Reviews 317, 108257, http://doi.org/10.1016/j.quascirev.2023.108257

Santamaría, M., Navazo, M., Arnold, L.J., Benito-Calvo, A., Demuro, M., Carbonell, E., 2023. Low-cost technologies in a rich ecological context: Hotel California open-air site at Sierra de Atapuerca, Burgos, Spain. Journal of Quaternary Science 38, 658-684, http://doi.org/10.1002/jqs.3501

Shipton, C., O'Connor, S., Jankowski, N., O'Connor-Veth, J., Maloney, T., Kealy, S., Boulanger, C., 2019. A new 44,000-year sequence from Asitau Kuru (Jerimalai), Timor-Leste, indicates long-term continuity in

human behaviour. Archaeological and Anthropological Sciences 11, 5717-5741, http://doi.org/10.1007/s12520-019-00840-5

Shtienberg, G., Yasur-Landau, A., Norris, R.D., Lazar, M., Rittenour, T.M., Tamberino, A., Gadol, O., Cantu, K., Arkin-Shalev, E., Ward, S.N., Levy, T.E., 2020. A Neolithic mega-tsunami event in the eastern Mediterranean: Prehistoric settlement vulnerability along the Carmel coast, Israel. PLOS ONE 15, e0243619, http://doi.org/10.1371/journal.pone.0243619

Smedley, R.K., Fenn, K., Stanistreet, I.G., Stollhofen, H., Njau, J.K., Schick, K., Toth, N., 2024. Age-depth model for uppermost Ndutu Beds constrains Middle Stone Age technology and climate-induced paleoenvironmental changes at Olduvai Gorge (Tanzania). Journal of Human Evolution 186, 103465, http://doi.org/10.1016/j.jhevol.2023.103465

Terradillos-Bernal, M., Demuro, M., Arnold, L.J., Jordá-Pardo, J.F., Clemente-Conte, I., Benito-Calvo, A., Díez Fernández-Lomana, J.C., 2023. San Quirce (Palencia, Spain): new chronologies for the Lower to Middle Palaeolithic transition of south-west Europe. Journal of Quaternary Science 38, 21-37, http://doi.org/10.1002/jqs.3460

Todisco, D., Mallol, C., Lahaye, C., Guérin, G., Bachellerie, F., Morin, E., Gravina, B., Challier, A., Beauval, C., Bordes, J.-G., Colange, C., Dayet, L., Flas, D., Lacrampe-Cuyaubère, F., Lebreton, L., Marot, J., Maureille, B., Michel, A., Muth, X., Nehme, C., Rigaud, S., Tartar, E., Teyssandier, N., Thomas, M., Rougier, H., Crevecoeur, I., 2023. A multiscalar and multiproxy geoarchaeological approach to site formation processes at the Middle and Upper Palaeolithic site of La Roche-à-Pierrot, Saint-Césaire, France. Quaternary Science Reviews 315, 108218, http://doi.org/10.1016/j.quascirev.2023.108218

Tsakalos, E., Efstratiou, N., Bassiakos, Y., Kazantzaki, M., Filippaki, E., 2021. Early Cypriot Prehistory: On the Traces of the Last Hunters and Gatherers on the Island—Preliminary Results of Luminescence Dating. Current Anthropology 62, 412-425, http://doi.org/10.1086/716100

Urbanová, P., Boaretto, E., Artioli, G., 2020. The state-of-the-art of dating techniques applied to ancient mortars and binders: A review. Radiocarbon 62, 503-525, http://doi.org/10.1017/RDC.2020.43

Vichaidid, T., Saeingjaew, P., 2022. Thermoluminescence and electron spin resonance dating of freshwater fossil shells from Pa Toh Roh Shelter archaeological site in southern Thailand. Heliyon 8, e10555, http://doi.org/10.1016/j.heliyon.2022.e10555

Wei, J., Jin, J., Hou, C., Xu, D., 2023. Prehistoric human activities and environmental background during the Late Neolithic to Bronze period in the Minjiang River Basin, Southeast China, based on luminescence ages and chemical elemental analysis of pottery. Quaternary Science Reviews 319, 108325, http://doi.org/10.1016/j.quascirev.2023.108325

ESR, applied in various contexts

Benito-Calvo, A., Moreno, D., Fujioka, T., López, G.I., Martín-González, F., Martínez-Fernández, A., Hernando-Alonso, I., Karampaglidis, T., Bermúdez de Castro, J.M., Gutiérrez, F., 2022. Towards the steady state? A long-term river incision deceleration pattern during Pleistocene entrenchment (Upper Ebro River, Northern Spain). Global and Planetary Change 213, 103813, http://doi.org/10.1016/j.gloplacha.2022.103813

Demeter, F., Zanolli, C., Westaway, K.E., Joannes-Boyau, R., Duringer, P., Morley, M.W., Welker, F., Rüther, P.L., Skinner, M.M., McColl, H., Gaunitz, C., Vinner, L., Dunn, T.E., Olsen, J.V., Sikora, M., Ponche, J.-L., Suzzoni, E., Frangeul, S., Boesch, Q., Antoine, P.-O., Pan, L., Xing, S., Zhao, J.-X., Bailey, R.M., Boualaphane, S., Sichanthongtip, P., Sihanam, D., Patole-Edoumba, E., Aubaile, F., Crozier, F., Bourgon, N., Zachwieja, A., Luangkhoth, T., Souksavatdy, V., Sayavongkhamdy, T., Cappellini, E., Bacon, A.-M., Hublin, J.-J., Willerslev, E., Shackelford, L., 2022. A Middle Pleistocene Denisovan molar from the Annamite Chain of northern Laos. Nature Communications 13, 2557, http://doi.org/10.1038/s41467-022-29923-z

Duval, M., Sahnouni, M., Parés, J.M., Zhao, J.-x., Grün, R., Abdessadok, S., Pérez-González, A., Derradji, A., Harichane, Z., Mazouni, N., Boulaghraief, K., Cheheb, R.C., van der Made, J., 2023. On the age of Ain Hanech Oldowan locality (Algeria): First numerical dating results. Journal of Human Evolution 180, 103371, http://doi.org/10.1016/j.jhevol.2023.103371

Freidline, S.E., Westaway, K.E., Joannes-Boyau, R., Duringer, P., Ponche, J.-L., Morley, M.W., Hernandez, V.C., McAllister-Hayward, M.S., McColl, H., Zanolli, C., Gunz, P., Bergmann, I., Sichanthongtip, P., Sihanam, D., Boualaphane, S., Luangkhoth, T., Souksavatdy, V., Dosseto, A., Boesch, Q., Patole-Edoumba, E., Aubaile, F., Crozier, F., Suzzoni, E., Frangeul, S., Bourgon, N., Zachwieja, A., Dunn, T.E., Bacon, A.-M., Hublin, J.-J., Shackelford, L., Demeter, F., 2023. Early presence of Homo sapiens in

Southeast Asia by 86–68 kyr at Tam Pà Ling, Northern Laos. Nature Communications 14, 3193, http://doi.org/10.1038/s41467-023-38715-y

Grün, R., Pike, A., McDermott, F., Eggins, S., Mortimer, G., Aubert, M., Kinsley, L., Joannes-Boyau, R., Rumsey, M., Denys, C., Brink, J., Clark, T., Stringer, C., 2020. Dating the skull from Broken Hill, Zambia, and its position in human evolution. Nature 580, 372-375, http://doi.org/10.1038/s41586-020-2165-4

Grün, R., Stringer, C., 2023. Direct dating of human fossils and the ever-changing story of human evolution. Quaternary Science Reviews 322, 108379, http://doi.org/10.1016/j.quascirev.2023.108379

Han, F., Bahain, J.-J., Shao, Q., Sun, X., Voinchet, P., Xiao, P., Huang, M., Li, M., Yin, G., 2022. The Chronology of Early Human Settlement in Three Gorges Region, China—Contribution of Coupled Electron Spin Resonance and Uranium-Series Dating Method. Frontiers in Earth Science 10, http://doi.org/10.3389/feart.2022.939766

Liu, C.-R., Tian, Y.-Y., Ji, H., Ma, X., Wei, C.-Y., Dang, J.-X., Yin, G.-M., Zhou, Y.-S., Yuan, R.-M., 2023. Chronology analysis of huge landslide based on ESR dating materials on sliding face in carbonate areas of south eastern Tibet. Quaternary Geochronology 76, 101442, http://doi.org/10.1016/j.quageo.2023.101442

Vichaidid, T., Saeingjaew, P., 2022. Thermoluminescence and electron spin resonance dating of freshwater fossil shells from Pa Toh Roh Shelter archaeological site in southern Thailand. Heliyon 8, e10555, http://doi.org/10.1016/j.heliyon.2022.e10555

Basic research

Ageby, L., Shanmugavel, J., Jain, M., Murray, A.S., Rades, E.F., 2024. Towards the optically stimulated luminescence dating of unheated flint. Quaternary Geochronology 79, 101471, http://doi.org/10.1016/j.quageo.2023.101471

Almeida, A.L.P.C., Tatumi, S.H., Soares, A.F., Barbosa, R., 2022. TL and OSL analysis of natural orange calcite crystal. Brazilian Journal of Radiation Sciences 10, 1-15, http://doi.org/10.15392/bjrs.v10i2A.1797

Bartz, M., Peña, J., Grand, S., King, G.E., 2023. Potential impacts of chemical weathering on feldspar luminescence dating properties. Geochronology 5, 51-64, http://doi.org/10.5194/gchron-5-51-2023

Buchanan, G.R., Tsukamoto, S., Zhang, J., Long, H., 2024. Testing infrared radiofluorescence dating on polymineral fine-grains from the Luochuan loess-palaeosol sequence, Chinese loess plateau. Quaternary Geochronology 79, 101485, http://doi.org/10.1016/j.quageo.2023.101485

Devi, M., Chauhan, N., Singhvi, A.K., 2024. Post-violet infrared stimulated luminescence (pVIRSL) dating protocol for potassium feldspar. Quaternary Geochronology 79, 101487, http://doi.org/10.1016/j.quageo.2023.101487

Duller, G.A.T., Roberts, H.M., Chapot, M.S., 2023. Characterising and correcting for a previously unconsidered source of scatter in measurements of equivalent dose. Radiation Measurements 167, 106985, http://doi.org/10.1016/j.radmeas.2023.106985

Freiesleben, T.H., Thomsen, K.J., Sellwood, E., Liu, J., Murray, A.S., 2023. Testing new kinetic models and calibration methods for Rock Surface Luminescence Exposure dating using controlled experiments. Radiation Measurements 169, 107033, http://doi.org/10.1016/j.radmeas.2023.107033

Goswami, K., Panda, S.K., Alappat, L., Chauhan, N., 2024. Luminescence for sedimentary provenance quantification in river basins: A methodological advancement. Quaternary Geochronology 79, 101488, http://doi.org/10.1016/j.quageo.2023.101488

Hou, C., Jin, J., Ling, Z., Wei, J., Xu, D., 2024. Spatio-temporal variation in quartz luminescence sensitivity in the coastal area of China. CATENA 234, 107585, http://doi.org/10.1016/j.catena.2023.107585

Lawless, J.L., Timar-Gabor, A., 2024. A new analytical model to fit both fine and coarse grained quartz luminescence dose response curves. Radiation Measurements 170, 107045, http://doi.org/10.1016/j.radmeas.2023.107045

Mandowska, E., Smyka, R., Mandowski, A., 2022. Investigating the filling state of OSL detector traps with the optical sampling method. Metrology and Measurement Systems 29, 361-371, http://doi.org/10.24425/mms.2022.140039

Pagonis, V., Polymeris, G.S., Kitis, G., Sahare, P.D., 2023. The effect of particle size on the radiation dose response of luminescence signals from nanophosphors. Radiation Measurements 166, 106965, http://doi.org/10.1016/j.radmeas.2023.106965

Riedesel, S., Duller, G.A.T., Ankjærgaard, C., 2023. Time-resolved infrared stimulated luminescence of the blue and yellow-green emissions – Insights into charge recombination in chemically and structurally different alkali feldspars. Journal of Luminescence 257, 119724, http://doi.org/10.1016/j.jlumin.2023.119724

Spooner, N.A., Williams, O.M., Questiaux, D.G., 2024. Pulsed infrared stimulated luminescence measurements for defect pair model studies in feldspars. Radiation Measurements 170, 107044, http://doi.org/10.1016/j.radmeas.2023.107044

Zhang, J., Li, S.-H., Sun, J., Lü, T., Zhou, X., Hao, Q., 2023. Quartz luminescence sensitivity variation in the Chinese loess deposits: the potential role of wildfires. Journal of Quaternary Science 38, 49-60, http://doi.org/10.1002/jqs.3462

Zhang, J., Tsukamoto, S., Long, H., 2023. Testing the potential of pulsed post-IR IRSL dating on Chinese loess deposits. Quaternary Geochronology 78, 101469, http://doi.org/10.1016/j.quageo.2023.101469

beyond quartz and K-feldspar: non-traditional minerals

- flint

Ageby, L., Shanmugavel, J., Jain, M., Murray, A.S., Rades, E.F., 2024. Towards the optically stimulated luminescence dating of unheated flint. Quaternary Geochronology 79, 101471, http://doi.org/10.1016/j.quageo.2023.101471

Dose rate

Martin, L., Sanderson, D.C.W., Paling, S., Cresswell, A., Fitzgerald, S.K., 2023. Quantitative beta autoradiography of a heterogeneous granulite sample and implications for luminescence dating. Radiation Measurements 168, 107001, http://doi.org/10.1016/j.radmeas.2023.107001

Preusser, F., Degering, D., Fülling, A., Miocic, J., 2023. Complex dose rate calculations in luminescence dating of lacustrine and palustrine sediments from Niederweningen, Northern Switzerland. Geochronometria 50, 28-49, http://doi.org/10.2478/geochr-2023-0003

Szymak, A., Moska, P., Poręba, G., Tudyka, K., Adamiec, G., 2022. The internal dose rate in quartz grains: Experimental data and consequences for luminescence dating. Geochronometria 49, 9-17, http://doi.org/10.2478/geochr-2022-0002

Tudyka, K., Koruszowic, M., Osadnik, R., Adamiec, G., Moska, P., Szymak, A., Bluszcz, A., Zhang, J., Kolb, T., Poręba, G., 2023. µRate: An online dose rate calculator for trapped charge dating. Archaeometry 65, 423-443, http://doi.org/10.1111/arcm.12828

Dosimetry

Almeida, A.L.P.C., Tatumi, S.H., Soares, A.F., Barbosa, R., 2022. TL and OSL analysis of natural orange calcite crystal. Brazilian Journal of Radiation Sciences 10, 1-15, http://doi.org/10.15392/bjrs.v10i2A.1797

Discher, M., Bassinet, C., Kim, H., 2023. Feasibility study of using earbuds and wireless headphones for retrospective dosimetry. Radiation Measurements 167, 107000, http://doi.org/10.1016/j.radmeas.2023.107000

Kara, E., Woda, C., 2023. Further characterization of BeO detectors for applications in external and medical dosimetry. Radiation Measurements 165, 106950, http://doi.org/10.1016/j.radmeas.2023.106950

Łepkowska, J., Jung, A., 2022. Influence of readout conditions on the thermoluminescence properties of mobile phone display glass for retrospective dosimetry. Measurement 204, 112083, http://doi.org/10.1016/j.measurement.2022.112083

Mahmood, M.M., Kakakhel, M.B., Wazir-ud-Din, M., Hayat, S., Ahmad, K., ur-Rehman, S., Siddique, M.T., Masood, A., ul-Haq, A., Mirza, S.M., 2022. Thermoluminescence (TL), kinetic parameters and dosimetric features of Pakistani limestone. Applied Radiation and Isotopes 188, 110357, http://doi.org/10.1016/j.apradiso.2022.110357

Motta, S., Christensen, J.B., Yukihara, E.G., 2023. Testing the S/SR procedure using TLDs and OSLDs and a lexsyg smart automated reader for precise dosimetry. Radiation Measurements 168, 107013, http://doi.org/10.1016/j.radmeas.2023.107013

Reimitz, D., Hupka, I., Ekendahl, D., 2022. OSL sensitivity of quartz extracted from fired bricks for retrospective dosimetry. Radiation Protection Dosimetry 198, 641-645, http://doi.org/10.1093/rpd/ncac111

Yukihara, E.G., 2023. TL and OSL as research tools in luminescence: Possibilities and limitations. Ceramics International 49, 24356-24369, http://doi.org/10.1016/j.ceramint.2022.10.199

Portable instruments

Esiana, B.O.I., Oram, R.D., 2023. Soil and spatial analyses in the assessment of the focal point of the extinct medieval royal burgh of Roxburgh. Journal of Archaeological Science: Reports 50, 104104, http://doi.org/10.1016/j.jasrep.2023.104104

Hudson, S.M., Waddington, C., Pears, B., Ellis, N., Parker, L., Hamilton, D., Alsos, I.G., Hughes, P., Brown, A., 2023. Lateglacial and Early Holocene palaeoenvironmental change and human activity at Killerby Quarry, North Yorkshire, UK. Journal of Quaternary Science 38, 403-422, http://doi.org/10.1002/jqs.3488

Nitundil, S., Stone, A., Srivastava, A., 2023. Applicability of using portable luminescence reader for rapid age-assessments of dune accumulation in the Thar desert, India. Quaternary Geochronology 78, 101468, http://doi.org/10.1016/j.quageo.2023.101468

Review

Feathers, J., 2023. The contributions of luminescence dating of sediments to understanding the first settlement of the Americas. PaleoAmerica 9, 81-114, http://doi.org/10.1080/20555563.2023.2234740

Gray, H.J., Jain, M., Sawakuchi, A.O., Mahan, S.A., Tucker, G.E., 2019. Luminescence as a Sediment Tracer and Provenance Tool. Reviews of Geophysics 57, 987-1017, http://doi.org/10.1029/2019RG000646

Grün, R., Stringer, C., 2023. Direct dating of human fossils and the ever-changing story of human evolution. Quaternary Science Reviews 322, 108379, http://doi.org/10.1016/j.quascirev.2023.108379

Urbanová, P., Boaretto, E., Artioli, G., 2020. The state-of-the-art of dating techniques applied to ancient mortars and binders: A review. Radiocarbon 62, 503-525, http://doi.org/10.1017/RDC.2020.43

Yukihara, E.G., 2023. TL and OSL as research tools in luminescence: Possibilities and limitations. Ceramics International 49, 24356-24369, http://doi.org/10.1016/j.ceramint.2022.10.199

Simulation and modelling

Guibert, P., Guérin, G., Javel, J.-B., Urbanová, P., 2020. Modeling light exposure of quartz grains during mortar making: Consequences for optically stimulated luminescence dating. Radiocarbon 62, 693-711, http://doi.org/10.1017/RDC.2020.34

Guyez, A., Bonnet, S., Reimann, T., Carretier, S., Wallinga, J., 2023. A novel approach to quantify sediment transfer and storage in rivers—testing feldspar single-grain pirir analysis and numerical simulations. Journal of Geophysical Research: Earth Surface 128, e2022JF006727, http://doi.org/10.1029/2022JF006727

Li, B., Jacobs, Z., Roberts, R.G., 2023. A Bayesian hierarchical age model for optical dating of single grains of quartz. Quaternary Geochronology 77, 101455, http://doi.org/10.1016/j.quageo.2023.101455

Peng, J., Li, B., Jacobs, Z., Andrew Gliganic, L., 2023. Optical dating of sediments affected by post-depositional mixing: Modelling, synthesizing and implications. CATENA 232, 107383, http://doi.org/10.1016/j.catena.2023.107383

Conference Announcements: 15th New World Luminescence Dating Workshop (NWLDW)

We are excited to announce that registration and abstract submission is now open for the **15th New World Luminescence Dating Workshop (NWLDW)** which is being held from **June 11-14, 2024** at the Desert Research Institute (DRI) in Reno, NV! **The abstract and registration deadlines are April 12th, 2024 and May 11th, 2024, respectively**. This workshop serves as a forum for luminescence practitioners to share their findings with the broader scientific community, and provides a friendly, inclusive venue for students to meet and interact with experts in the field.

Registration is $100 for professionals and free for students presenting an oral or poster presentation, courtesy of the Roxie and Joseph Azad Foundation. Registration for non-presenting students is at a discounted rate of $50. Our (optional) conference dinner will be held on the evening of June 12th, 2024 at the Wild River Grille in downtown Reno. The cost of the conference dinner is $50 for professionals, $30 for student non-presenters, and free for student presenters.

To register and submit your abstract, please visit the NWLDW 2024 website. Additional information including a preliminary meeting and field trip schedule can also be found on the NWLDW 2024 website.

Hotel rooms fill up quickly in the summer months, so we strongly suggest securing accommodation as soon as possible if you plan to attend the workshop. In Reno, we recommend two hotels that are both located conveniently in the downtown core of the city and are within walking distance of our conference dinner venue:

- Whitney Peak Hotel
- Renaissance Hotel

There are a limited number of openings available for the field trip (max number of participants is 30), so please register early to secure your spot! For those planning to attend the field trip, we encourage you to secure accommodation in Tahoe City, California as soon as possible. We recommend Granlibakken Tahoe, but there are several other options in the Tahoe City area.

Please get in touch with us at drill@dri.edu if you have any questions. Looking forward to seeing you there!

Best,
Kathleen, Christina, and Amanda

Ancient TL

ISSN 2693-0935

Aims and Scope

Ancient TL is a journal devoted to Luminescence dating, Electron Spin Resonance (ESR) dating, and related techniques. It aims to publish papers dealing with experimental and theoretical results in this field, with a minimum of delay between submission and publication. Ancient TL also publishes a current bibliography, thesis abstracts, letters, and miscellaneous information, e.g., announcements for meetings.

Frequency

Two issues per annum in June and December

Submission of articles to Ancient TL

Ancient TL has a reviewing system in which direct dialogue is encouraged between reviewers and authors. For instructions to authors and information on how to submit to Ancient TL, please visit the website at:
http://ancienttl.org/TOC1.htm

Journal Enquiries

For enquiries please contact the editor:
Regina DeWitt, Department of Physics, East Carolina University, Howell Science Complex, 1000 E. 5th Street, Greenville, NC 27858, USA; Tel: +252-328-4980; Fax: +252-328-0753 (dewittr@ecu.edu)

Subscriptions to Ancient TL

Ancient TL Vol. 32 No.2 December 2014 was the last issue to be published in print. Past and current issues are available for download free of charge from the Ancient TL website:
http://ancienttl.org/TOC4.htm